Supplementary Information:

Enhancing plasma-based cracking of NH_3 : the beneficial effect of N_2 versus the detrimental effect of H_2

Seunghwan Bang^{a,b*} and Ramses Snoeckx^{a,c}

^{a.} CERP, Physical Science and Engineering Division (PSE), King Abdullah University of Science and Technology (KAUST), Thuwal 23955, Saudi Arabia

^{b.} Research group PLASMANT, Department of Chemistry, University of Antwerp, Universiteitsplein 1, BE-2610 Wilrijk-Antwerp, Belgium

^{c.} Laboratory for Advanced Fibers, Empa, Swiss Federal Laboratories for Materials Science and Technology, Lerchenfeldstrasse 5, 9014 St. Gallen, Switzerland

1. Experimental details

The experimental system comprised four main components: a reactant supply, a temperature-controlled dielectric barrier discharge (DBD) reactor, a power delivery unit, and an analysis section (Figure S1). Mass flow rates of NH₃ (99.98%), N₂ (99.999%), and H₂ (99.99%) were regulated by three mass flow controllers (Brooks, SLA5850). For the standard operating condition, the total flow rate was fixed at 200 SCCM for all mixture compositions of NH₃, N₂ and H₂. The reactor pressure was maintained at 1 atm.

The temperature-controlled DBD reactor consisted of a quartz flow tube (length: 850 mm; outer diameter: 60 mm; inner diameter: 54 mm) placed inside an electric furnace. The reactor included a 330 mm pre-heating zone, which ensured that the inlet gas mixture reached the target temperature (T_g) before entering the discharge zone. The systematic error of the furnace temperature relative to T_g inside the reactor was estimated to be ± 15 K because additional heating due to plasma operation was checked by measuring the gas temperature with a K-type thermocouple positioned 3 cm downstream of the discharge zone. This temperature rise remained below 22.7 K for a pure N_2 plasma (see Figure S6 in Section S2.2).

^{*}Corresponding author: seunghwan.bang@uantwerp.be

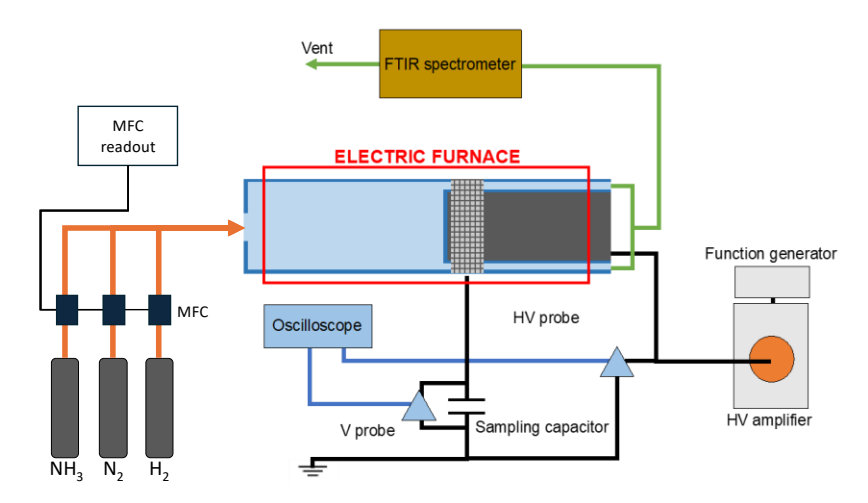


Figure S1. Schematic of the experimental setup.

The DBD region had a 2 mm gas gap formed by an inner quartz tube (length: 380 mm; O.D.: 50 mm; I.D.: 46 mm) placed concentrically inside the outer tube. A stainless-steel sheet (1 mm thick, 380 mm long) attached to the inner wall of the inner tube served as the high-voltage (HV) electrode. The grounded electrode was a stainless-steel mesh, 40 mm wide, wrapped around the outer quartz tube, giving a discharge volume of 13.1 cm³. Both the HV and ground electrodes were covered by quartz barriers. This minimized catalytic effects from exposed metallic surfaces, which is particularly important for NH₃ decomposition, since metals are known to catalyze NH₃ dissociation.

The plasma was powered by a high-voltage amplifier (Trek 30/20 A) driven by a sinusoidal waveform from a function generator (Tektronix AFG 3021B). The applied voltage at the HV electrode and the voltage across a 10 nF sampling capacitor were monitored using voltage probes (Tektronix P6015A and TPP1000) connected to a digital oscilloscope (Tektronix DPO 4140B). The discharge power ($P_{\rm dis}$) was determined from the area of the Q–V (Lissajous) plot.

For product analysis, the reactor outlet was connected to an inline Fourier-transform infrared spectrometer (FTIR, Thermo Fisher Scientific Nicolet iS10) equipped with a 2 m gas cell. The mole fraction of NH₃ (x_{NH_3}) was quantified as a measure of NH₃ decomposition into H₂ and N₂. The FTIR method had a systematic uncertainty of ± 1.5 % (on the order of several hundred ppm), independent of operating conditions and number of repetitions.

The NH₃ conversion ($X_{\rm NH_3}$) was defined on the basis of $X_{\rm NH_3}$ as follows:

$$X_{NH_3} \left[\%\right] = \frac{A_{NH_3@plasma.off} - A_{NH_3@plasma.on}}{A_{NH_3.@plasma.ff} + (A_{NH_3@plasma.off} \times A_{NH_3@plasma.on})}$$

, where $A_{NH_3.@plasma.off}$ and $A_{NH_3.@plasma.on}$ stand for area of NH₃ peak from FTIR spectrum when plasma is on and off, respectively. Note that the nominator is not simply $A_{NH_3.@plasma.off}$ to compensate the gas expansion due to NH₃ cracking and this is valid only when all NH₃ molecules cracked become N₂ and H₂, no other by-products (e.g., N₂H₄).

The H₂ production rate, shown in Figure 1, was calculated as:

$$H_2$$
 production rate $[Nml/min] = X_{NH_3} \times \dot{Q}_{initial.NH_3} \times 1.5$

, where $\dot{Q}_{initial.NH_3}$ is the initial flow rate of NH₃, and the factor 1.5 accounts for the 1.5 mole of H₂ contained in one mole of NH₃.

The energy cost (EC) listed in Table 1 in the manuscript was obtained by:

$$EC [eV/molecule] = \frac{SEI}{(X_{NH_3} \div 100\%)}$$

, herein SEI is the specific energy input in eV/molecule converted from J/cm³, SEI = $P_d/\dot{Q}_{initial}$.

A schematic representation of the experimental setup is given in Figure S1. The experimental procedure consisted of (i) stabilizing the gas temperature, T_g , for 40 minutes, (ii) turning on the discharge and waiting for 15 minutes to make sure the discharge has stabilized, (iii) taking 5 consecutive measurements of NH₃ with the Fourier Transform InfraRed spectroscope (FTIR, Thermo Fischer Scientific, Nicolet iS10), which takes 60 ± 5 seconds per measurement including the electrical measurement, (iv) turning off the discharge and raising T_g for the next measurement, and (v) repeating the steps above (i–iv). The NH₃ conversion results were thus the average of 5 consecutive measurements. All measurements were performed for a fixed mixture of NH₃, N₂ and H₂ at a fixed total flow rate, while the applied AC voltage adjusted the discharge power with a fixed AC frequency at 2.5 kHz.

Due to the abrupt reduction of the cross-sectional area, a velocity profile at the inlet of the DBD section should be close to a uniform one and transform into a parabolic one (because the flow was in laminar regime for all tested conditions, Re < 100) as the flow passed through a thin annular gap. However, the

flow was significantly disturbed due to many discharge filaments and an ionic wind. Considering that the ionic wind blows in the radial direction primarily and the radial gap distance is only 2 mm, intense mixing could flatten out the radial concentration profile as well as the radial velocity profile. Thus, the effect of DBD on the flow and concentration profile prevails over that of the reduction in the cross-sectional area. In this regard, we believe that the difference in the cross-sectional area between the preheating and the DBD sections would not cause a significant issue for 0D approximation.

1.1. Measured H₂ production rate and NH₃ conversion

The following tables give the experimental data for the different experimental cases.

Tables S1–S3 contain the data used for Figure 1 in the main manuscript.

Table S1. The measured H_2 production rate (NmI- H_2 /min), energy yield (mol/J), NH₃ conversion (%), and energy cost (eV/molecule-NH₃) for the cases at $T_g = 600$ K, SEI = 6 J/cm³ ($P_{dis} = 20$ W), and flow rate of 200 SCCM. The tested mixture contained NH₃ and a N₂/H₂ mixture with a 1:3 ratio of N₂ to H₂.

NH ₃ concentration (v/v%)	H ₂ Production rate (Nml-H ₂ /min)	Energy yield (Nml-H ₂ /J)	NH ₃ conversion (%)	Energy cost (eV/molecule-NH ₃)
100	7.20	1.200	2.40	58
90	4.33	0.722	1.60	97
75	3.87	0.645	1.72	108
50	2.93	0.488	1.95	143
25	1.05	0.175	1.40	398
10	0.59	0.098	1.97	709

Table S2. The measured H_2 production rate (NmI- H_2 /min), energy yield (mol/J), NH₃ conversion (%), and energy cost (eV/molecule-NH₃) for the cases at $T_g = 600$ K, SEI = 6 J/cm³ ($P_{dis} = 20$ W), and flow rate of 200 SCCM. The tested mixture contained NH₃ and N₂.

NH ₃ concentration (v/v%)	H ₂ Production rate (Nml-H ₂ /min)	Energy yield (Nml-H ₂ /J)	NH ₃ conversion (%)	Energy cost (eV/molecule-NH ₃)
100	7.20	1.200	2.40	58
90	5.07	0.845	1.88	82
75	3.41	0.568	1.52	123
50	4.85	0.808	3.23	86
25	6.69	1.115	8.92	62
10	4.61	0.768	15.4	91

Table S3. The measured H_2 production rate (NmI- H_2 /min), energy yield (mol/J), NH₃ conversion (%), and energy cost (eV/molecule-NH₃) for the cases at $T_g = 600$ K, SEI = 6 J/cm³ ($P_{dis} = 20$ W), and flow rate of 200 SCCM. The tested mixture contained NH₃ and H₂.

NH ₃ concentration (v/v%)	H ₂ Production rate (Nml-H ₂ /min)	Energy yield (Nml-H ₂ /J)	NH ₃ conversion (%)	Energy cost (eV/molecule-NH ₃)
100	7.20	1.200	2.40	58
90	3.88	0.647	1.44	108
75	3.50	0.583	1.56	119
50	2.80	0.467	1.87	150
25	0.68	0.113	0.91	619
10	0.28	0.047	0.93	1488

Tables S4–S6 contain the data used for Figure 2a (thermal cracking) in the main manuscript.

Table S4. The measured H_2 production rate (NmI- H_2 /min) and NH₃ conversion (%) for the cases at SEI = 0 J/cm³ ($P_{dis} = 0$ W). The tested mixture consisted of 1 v/v% NH₃ and 99 v/v% N₂/H₂ mixture in a 1:3 ratio. The flow rate was fixed at 1 SLPM.

Gas temperature (K)	H ₂ Production rate (Nml-H ₂ /min)	NH ₃ conversion (%)	
1000	0.0	0.0	
1100	0.0	0.0	
1200	0.0	0.0	
1300	0.0	0.0	
1350	0.0	0.0	
1400	0.0	0.0	
1450	0.0	0.0	

Table S5. The measured H₂ production rate (Nml-H₂/min) and NH₃ conversion (%) for the cases at SEI = 0 J/cm³ ($P_{dis} = 0$ W). The tested mixture consisted of 1 v/v% NH₃ and 99 v/v% N₂. The flow rate was fixed at 1 SLPM.

Gas temperature (K)	H ₂ Production rate (Nml-H ₂ /min)	NH ₃ conversion (%)	
1000	0.00	0.0	
1100	0.00	0.0	
1200	0.00	0.0	
1300	0.00	0.0	
1350	0.27	1.8	
1400	0.69	4.6	
1450	2.25	15.0	

Table S6. The measured H_2 production rate (Nml- H_2 /min) and NH₃ conversion (%) for the cases at SEI = 0 J/cm³ ($P_{dis} = 0$ W). The tested mixture consisted of 1 v/v% NH₃ and 99 v/v% H₂. The flow rate was fixed at 1 SLPM.

Gas temperature (K)	H ₂ Production rate (Nml-H ₂ /min)	NH ₃ conversion (%)		
1000	0.0	0.0		
1100	0.0	0.0		
1200	0.0	0.0		
1300	0.0	0.0		
1350	0.0	0.0		
1400	0.0	0.0		
1450	0.0	0.0		

Tables S7–S9 contain the data used for Figure 2b (plasma-based cracking) in the main manuscript.

Table S7. The measured H_2 production rate (Nml- H_2 /min), energy yield (mol/J), NH₃ conversion (%), and energy cost (eV/molecule-NH₃) for the cases at SEI = 1.2 J/cm³ (P_{dis} = 20 W). The tested mixture consisted of 1 v/v% NH₃ and 99 v/v% N₂/H₂ mixture in a 1:3 ratio. The flow rate was fixed at 1 SLPM.

Gas temperature (K)	H ₂ Production rate (Nml-H ₂ /min)	Energy yield (Nml-H ₂ /J)	NH ₃ conversion (%)	Energy cost (eV/molecule-NH ₃)
300	0.0	0.0	0.0	-
400	0.0	0.0	0.0	-
500	0.0	0.0	0.0	-
600	0.0	0.0	0.0	-
700	0.0	0.0	0.0	-
800	0.0	0.0	0.0	-
900	0.0	0.0	0.0	-

Table S8. The measured H₂ production rate (NmI-H₂/min), energy yield (mol/J), NH₃ conversion (%), and energy cost (eV/molecule-NH₃) for the cases at SEI = 1.2 J/cm³ (P_{dis} = 20 W). The tested mixture consisted of 1 v/v% NH₃ and 99 v/v% N₂. The flow rate was fixed at 1 SLPM.

Gas temperature (K)	H ₂ Production rate (Nml-H ₂ /min)	Energy yield (Nml-H ₂ /J)	NH ₃ conversion (%)	Energy cost (eV/molecule-NH ₃)
300	0.99	0.825	6.6	422
400	1.19	0.992	7.9	353
500	1.63	1.358	10.9	256
600	2.54	2.117	16.9	165
700	1.86	1.550	12.4	225
800	2.04	1.700	13.6	205
900	2.37	1.975	15.8	176

Table S9. The measured H_2 production rate (NmI- H_2 /min), energy yield (mol/J), NH₃ conversion (%), and energy cost (eV/molecule-NH₃) for the cases at SEI = 1.2 J/cm³ (P_{dis} = 20 W). The tested mixture consisted of 1 v/v% NH₃ and 99 v/v% H₂. The flow rate was fixed at 1 SLPM.

Gas temperature (K)	H ₂ Production rate (Nml-H ₂ /min)	Energy yield (Nml-H ₂ /J)	NH ₃ conversion (%)	Energy cost (eV/molecule-NH ₃)
300	0.0	0.0	0.0	-
400	0.0	0.0	0.0	-
500	0.0	0.0	0.0	-
600	0.0	0.0	0.0	-
700	0.0	0.0	0.0	-
800	0.0	0.0	0.0	-
900	0.0	0.0	0.0	-

1.2. Reduced electric field (E/N) and discharge mode (β)

In non-thermal plasmas, most of the electrical energy primarily goes to electrons due to the Lorentz force exerted by the applied electric field (E). These electrons move along the electric field transferring energy to other particles through collisions. The average distance between these collisions (mean free path) is constrained by the number density (N). As a result, the reduced electric field (E/N) determines the Electron Energy Distribution Function (EEDF) and the mean electron energy (T_e). Therefore, the reduced electric field is a key parameter for both the physical and chemical aspects of non-thermal plasmas. In general, it is not that straightforward to determine E/N for electrical discharges. However, for a DBD with a gas gap distance (d), a breakdown voltage (V_b) can be found from a QV-plot, which allows to estimate the electric field ($E \approx V_b/d$). Finally, E can be divided by N (obtained from the ideal gas law using the pressure and temperature) to yield E/N. The relative standard deviation on the measured E/N values is ± 1 %, which causes negligible variations (± 0.5 %) in terms of observed NH₃ conversion trend (see Figure S2). Measured E/N values are presented in Table S10 and S11 as well as Figure S3 and S4.

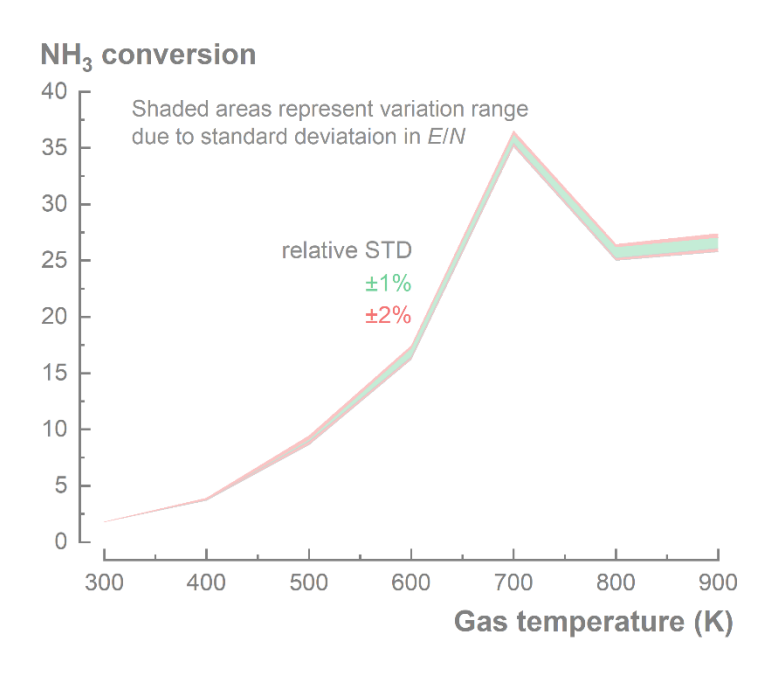


Figure S2. The variation in NH₃ conversion obtained from the simulations, taking into account the relative standard deviation of the measured *E/N* values, is negligible. Green shaded area represents the cases for a deviation of 1%, and red shaded area for a deviation of 2%.

As the NH₃ concentration decreases (at a fixed gas temperature of $T_g = 600$ K), E/N decreases (Table S10 and Figure S3), independent of the balance gas in the mixture. Starting at 100 v/v% NH₃ E/N = 200 Td and drops to ~187 Td at 90 v/v% NH₃ for all mixture conditions. As the NH₃ concentration decreases further, E/N in the NH₃/N₂ mixture decreases less than for the other two mixtures. The values of E/N for the other two mixtures are similar to each other and only differ significantly at 10 v/v% NH₃ (162 Td for NH₃/N₂/H₂ and 154 for NH₃/H₂).

When we look at E/N for the 1 v/v% NH₃ concentration cases (Table S11 and Figure S4a), as we vary the gas temperature from $T_g = 300$ to 900 K, nonlinear increasing trends of E/N are observed with maxima at $T_g = 700$ K. While linear increase in E/N is expected due to the relation $N \sim 1/T_g$, nonlinear increasing trend is the result of significant changes in V_b (Figure S4b). The observed nonlinear variation of V_b could be the result of different effects. First, Paschen's law describes the correlation between V_b and the product of the pressure (P) and the gap distance (d), $V_b \sim Pd$. Using the number density ($N \sim P$), this expression becomes $V_b \sim Nd$ for fixed pressure with varied T_g . As T_g increases from $T_g = 300$ K to 600 K, the decreased N leads to the initial decrease in V_b . Second, the properties of the dielectric material, such as a temperature-dependent resistance as well as permittivity, 5 could also influence the observed changes in V_b . However, the non-linear changes in V_b upon increased T_g requires further investigation in the future.

The discharge mode in a DBD reactor could provide insights for further optimization of the process because stronger micro-discharges, are believed to improve cracking of NH₃ and N₂ molecules; therefore, the representative parameter β (0 < β < 1) was calculated. A value of β = 1 corresponds to a uniform plasma occupying the entire discharge volume, whereas smaller values approaching zero indicate more localized, and thus stronger, micro-discharges. The equation used to calculate β is as follows:

$$\beta = \frac{\zeta_{diel} - C_{cell}}{C_{diel} - C_{cell}}$$

,where ζ_{diel} is the measured dielectric capacitance of the dielectric material, C_{diel} is the actual dielectric capacitance, and C_{cell} is the capacitance of the entire system. Since the DBD reactor has a cylindrical configuration, C_{diel} can be calculated as:

$$C_{diel} = \frac{2\pi\varepsilon L}{\ln(b/a)}$$

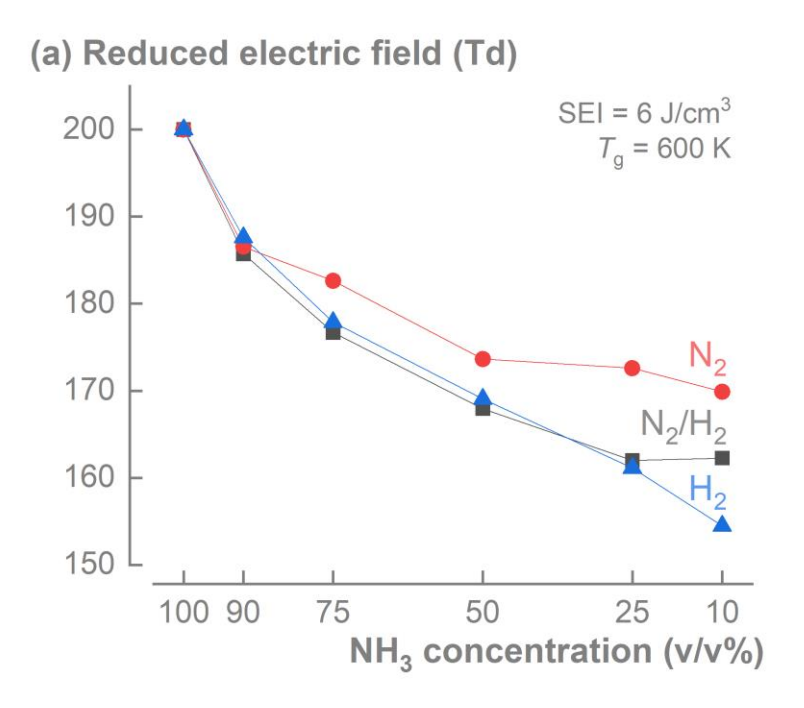
,where ε is the permittivity of the dielectric material, L is a length of discharge zone, and b and a denote the outer and inner diameters, respectively. In this study, ε was assumed constant and β values were calculated up to $T_g = 500$ K because detailed dielectric information (e.g., the crystallographic c-axis of quartz) is not available, although it is known to strongly affect the temperature dependence⁶. The assumption of constant ε is valid at least up to 570 K⁶, and thus can be used to give an indication of the discharge mode in our reactor.

Table S10. The measured breakdown voltage and reduced electric field for various NH₃ concentration ([NH₃]) and mixture conditions at $T_g = 600$ K, SEI = 6 J/cm³ ($P_{dis} = 20$ W and flow rate of 200 SCCM). The applied AC voltage adjusted the discharge power with a controlled AC frequency at 2.5 kHz. The tested mixture consisted of NH₃ and a gas mixture with (i) a 1:3 molar ratio of N₂ to H₂, (ii) pure N₂, and (iii) pure H₂ (corresponding to Figure S3).

	NH ₃ /N ₂ /H ₂		NH_3/N_2		NH ₃ /H ₂	
$[NH_3] - (v/v\%)$	V _b (V)	E/N (Td)	V _b (V)	<i>E/N</i> (Td)	V _b (V)	<i>E/N</i> (Td)
100	5000	200	-	-	-	-
90	4650	186	4675	187	4700	188
75	4425	177	4575	183	4450	178
50	4200	168	4350	174	4225	169
25	4050	162	4325	173	4025	161
10	4050	162	4250	170	3850	154

Table S11. The measured breakdown voltage, reduced electric field, and representative parameter for discharge mode (β) ⁷ for various T_g and mixture conditions at $T_g = 600$ K, SEI = 1.2 J/cm³ ($P_{dis} = 20$ W and flow rate of 1 SLPM). The applied AC voltage adjusted the discharge power with a controlled AC frequency at 2.5 kHz. The tested mixture consisted of 1% NH₃ and 99% gas mixture with (i) a 1:3 molar ratio of N₂ to H₂, (ii) N₂, and (iii) H₂ (corresponding to Figure S4). Only values of β below 500 K are reported, because the theoretical method of Peeters and van de Sanden⁷ is not applicable at higher temperatures. In reality, the actual capacitance can vary with increasing gas temperature, since the dielectric constant is known to rise sharply above ~600 K⁶. Nevertheless, the obtained β value of ~0.16 indicates that the micro-discharges in our reactor are relatively diffuse.

	NH ₃ /N ₂ /H ₂				NH_3/N_2			NH_3/H_2		
$T_{g}(\mathbf{K})$	$V_{ m b}$	E/N	β	$V_{ m b}$	E/N	β	$V_{ m b}$	E/N	β	
	(V)	(Td)		(V)	(Td)		(V)	(Td)		
300	4550	91	0.21	5100	102	0.16	4250	85	0.17	
400	3900	104	0.24	4613	123	0.20	3713	99	0.19	
500	3840	128	0.27	4290	143	0.23	3570	119	0.21	
600	4325	173	-	4100	164	-	3625	145	-	
700	5893	275	-	5164	241	-	5786	270	-	
800	4969	265	-	3525	188	-	4556	243	-	
900	4250	255	-	2650	159	-	3717	223	-	



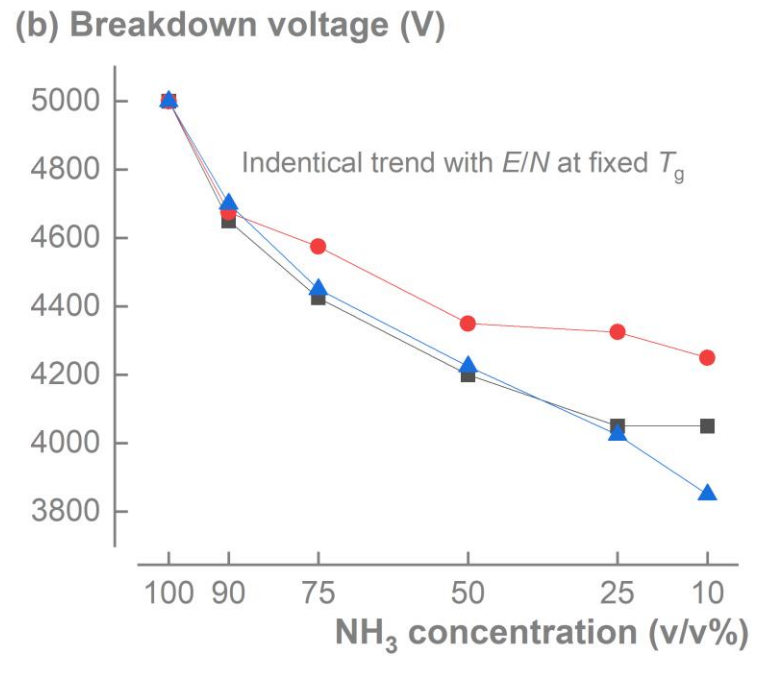
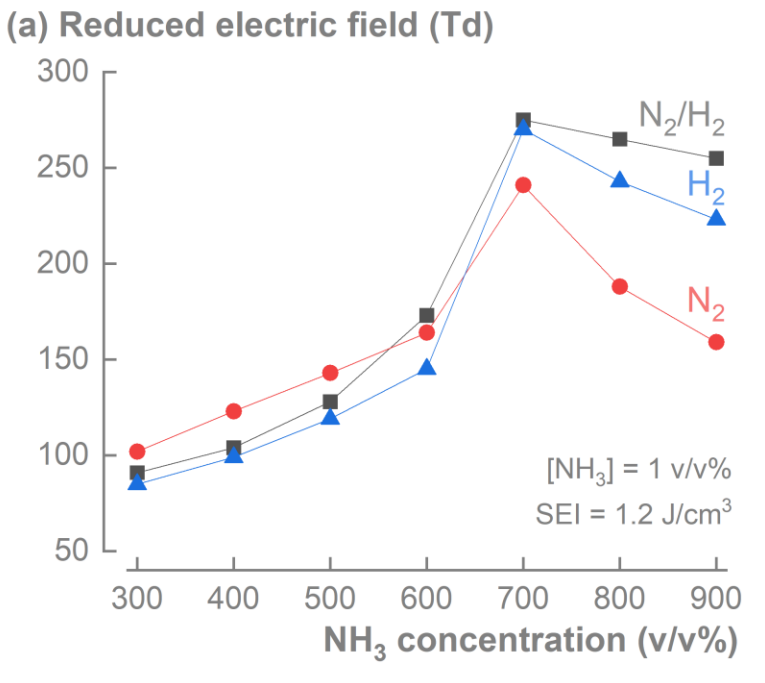


Figure S3. Electrical characteristics during plasma-based NH₃ cracking at gas temperature (T_g) of 600 K and specific energy input (SEI) of 6 J/cm³ (P_{dis} = 20 W at flow rate of 200 SCCM) across various NH₃ concentrations from 100 to 10 v/v%: (a) reduced electric field (E/N) and (b) breakdown voltage (V_b). The trends of E/N and V_b exhibit similar behavior. The tested mixture consisted of 1 v/v% NH₃ and (i) a 1:3 molar ratio of N₂ to H₂ (black), (ii) N₂ (red), and (iii) H₂ (blue).



(b) Breakdown voltage (V)

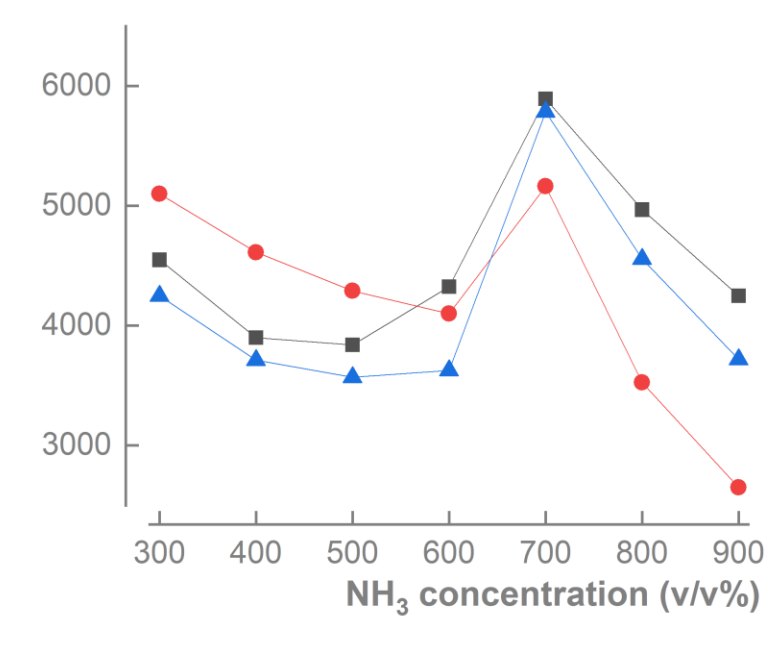


Figure S4. Electrical characteristics during plasma-based NH₃ cracking at constant NH₃ concentration of 1 v/v% and specific energy input (SEI) of 1.2 J/cm³ ($P_{dis} = 20$ W at flow rate of 1 SLPM) across gas temperatures from 300 to 900 K: (a) reduced electric field (E/N) and (b) breakdown voltage (V_b). A notable increase in E/N is observed between 600 and 700 K, consistent with the findings reported in ⁸. The tested mixture consisted of 1 v/v% NH₃ and (i) a 1:3 molar ratio of N₂ to H₂ (black), (ii) N₂ (red), and (iii) H₂ (blue).

2. Modeling details

2.1. Modeling the filamentary behavior/micro-discharges in the DBD

We mimicked the filamentary behavior of the dielectric barrier discharge by applying periodic rectangular micro-discharge pulses with a constant reduced electric field strength. In practice, the reduced electric field is not constant; it varies along the streamer, being strongest at the streamer front and then rapidly decreasing. As a result, the temporal profile of E/N typically shows a sharp spike followed by a relatively long plateau at lower values^{9–11}. To the best of our knowledge, accurate measurement of E/N in a DBD reactor has not yet been achieved, although several groups are actively developing advanced laser diagnostics for this purpose^{12–14}. In our specific setup, the temperature-controlled DBD reactor is enclosed by an electrical furnace, which further restricts optical access and makes direct measurement particularly challenging.

For these reasons, our model relies on the nominal E/N value estimated from the breakdown field using Q–V plots. Although this approach does not capture the complete temporal dynamics of E/N during a micro-discharge, it provides a practical basis for analyzing first-order trends in plasma chemical kinetics, as demonstrated in previous publications^{8,15–18}.

For the conditions under study, we assumed that each gas molecule passes through 288 micro-discharges for the given residence time. This number was chosen based on modeling results for various gas conversion process, such as ozone production¹⁶ and H₂ oxidation^{17,18}. And the simulation results for NH₃ cracking shows that, like O₃ production and H₂ conversion, the NH₃ conversion also becomes independent of the number of micro-discharges at 288 pulses (Figure S5). For instance, the simulation with 50 micro-discharges yields 18 % conversion, whereas 200 and 400 micro-discharges result in 17 % and 16.8 % conversion, respectively. These values are essentially identical to the case with 288 micro-discharges (16.9 %), with a relative error below 0.3%. Although not directly comparable due to differences in reactor geometry and reactants, the experimental study on CO₂ conversion by Ozkan et al.¹⁹ indirectly supports our choice, as it reported an average of 200–400 discharge channels. The power deposited in the system per micro-discharge was fixed and equal to the power delivered to the plasma divided by the total number of micro-discharges.

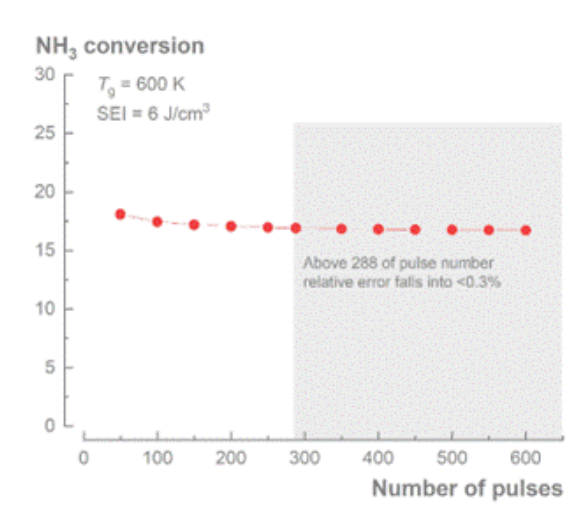


Figure S5. The NH $_3$ conversion as a function of the number of micro-discharges applied in the simulation. The gas temperature and SEI were fixed at 600 K and 6 J cm $^{-3}$, respectively. The results show that the conversion can be considered completely independent of the number of discharges. Once the value exceeds 288, the relative error is less than 0.3 %.

According to the literature, in DBDs, the plasma volume (i.e., the fraction of the reactor volume actually occupied by micro-discharges) is typically on the order of 0.1-1 %, and in some cases in the order of 10 %, depending on the operating conditions $^{8,17,18,20-23}$. In our case, electrical measurements indicate that the discharge in our DBD reactor is relatively diffuse, filling 16-27 % of the discharge zone of the reactor (as presented in Table S10 and S11). Note that the discharge mode was identified using the β parameter, a theoretical value derived from the Q–V plot as proposed by Peeters and Sanden 7 . These results suggest that we have both temporally and spatially distributed filaments, which only occupy a small portion of the total reactor volume. The power density obtained from our model was multiplied by a factor of 2 to match the SIE (Specific Input Energy) from the experiments, similar to the work of Aerts et al... As described by Aerts et al. "... even if this factor can be considered as a kind of fitting parameter, it does have a physical meaning as demonstrated by Motret et al... 20,21 Even if the quantitative calculation results might be dependent on this factor, the qualitative trends predicted by the model can still be validated in this way, and the validated model can subsequently be used to elucidate the underlying plasma chemistry". 22

2.2. Heating effects

The model considered three different zones corresponding to the different zones in the experimental setup (see Figure S1): (i) a preheating period (zone) with a controlled gas temperature and no applied electric field strength, corresponding to the experimental residence time in the "heating section" (ii) a discharge period (zone), where the rectangular micro-discharge pulses are applied, corresponding to the experimental residence time in the "discharge section", and (iii) a post plasma period (zone) with a controlled gas temperature and no applied electric field strength.

For the conditions with 1 v/v% NH₃ in 99 v/v% N₂ under study, we measured the difference in gas temperature (3-cm downstream of the DBD section) with and without turning on the DBD, and found that all measurement fell in $\Delta T_g < 22.7$ K, as Figure S6 as follows:

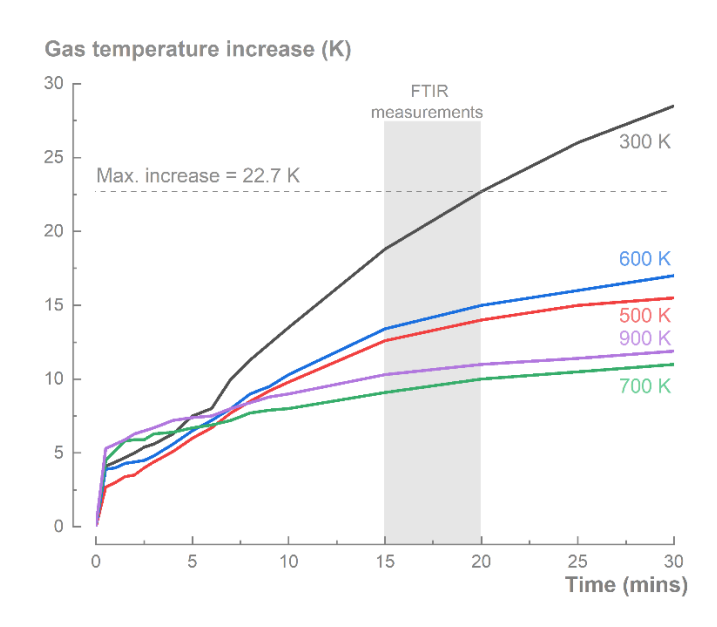


Figure S6. Temperature increase due to gas heating via electrical discharges in the furnace.

This observation is supported by the work by Jidenko et al.²⁴ and Motret et al..²¹ In both studies, only minimal increases in the gas temperature due to Joule heating were reported. Below a frequency of 10 kHz, Jidenko et al. found that the temperature at the discharge filaments was approximately 80 K higher than the surrounding gas temperature.²⁴ Similarly, Motret et al. found a general increase in the gas temperature of 30–50 K, for a high energy pulsed system (180 kV, 1 J/pulse, 100 cm³/min flow of Ar).²¹ Given the lower frequency and lower energy used in our study, the effect of Joule heating should indeed be lower than 30 K. Because N₂ is known to induce rapid gas heating through vibrational—translational

(VT) relaxation²⁵, whereas no comparable effect has been reported for the other species, the other gas compositions examined in this study are expected to exhibit smaller increases in gas temperature.

Changes in the effective heating length or heating rate might possibly shift the experimental data with respect to T_g . However, due to the low reactivity of NH₃, this effect can be expected to be insignificant for the tested range of T_g . To confirm this assumption, we performed simulations with the newly-present reaction mechanism in this study by changing the original residence time by a factor of 0.5 and 2. Even with these large variations, the observed shift in the onset temperature was ~50 K. This implies the modeling of plasma-based NH₃ cracking process can be regarded as an isothermal process.

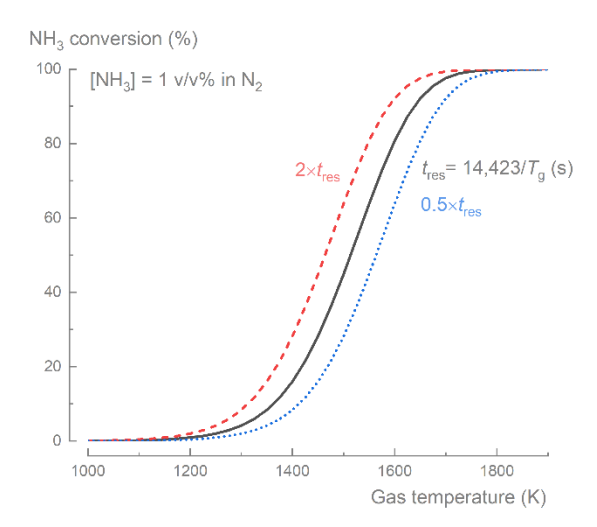


Figure S7. Effect of the residence time on NH₃ conversion as a function of T_g for the conventional (thermal) pyrolysis of NH₃. The mixture condition is 1 v/v% NH₃ in 99 v/v% N₂. The residence time corresponds to the value from experiment at flowrate = 1 SLPM.

2.3. Model input details

Table S12. Input parameters for the different modeling conditions.

	<i>E/N</i> (Td)			Residence time	# Discharge	Inter-pulse
$T_{\mathrm{g}}\left(\mathbf{K}\right)$	NH ₃ /N ₂ /H ₂	NH ₃ /N ₂	NH ₃ /H ₂	discharge zone	pulses	time (ms)
				(s)		
300	91	102	85	0.784	288	2.723
400	104	123	99	0.588	288	2.042
500	128	143	119	0.470	288	1.634
600	173	164	145	0.392	288	1.361
700	275	241	270	0.336	288	1.167
800	265	188	243	0.294	288	1.021
900	255	159	223	0.261	288	0.908

2.4. Modeling results

In this section, the results from the zero-dimensional chemical kinetic model are given, for both the previously published reaction mechanism ⁸ (Old mechanism) and the updated mechanism used in this work (New mechanism).

Table S13. The calculated NH₃ conversion via thermal-based NH₃ cracking at SEI = 0 J/cm³ and different gas temperatures (from 1000 K to 2500 K). The tested mixtures are 1 v/v% NH₃ in 99 v/v% N₂/H₂ mixture; 99 v/v% N₂, and 99 v/v% H₂ mixture (corresponding to Figure S8).

	Old mechanism			New mechanism			
$T_{ m g}$	NH ₃ /N ₂ /H ₂	NH ₃ /N ₂	NH ₃ /H ₂	NH ₃ /N ₂ /H ₂	NH ₃ /N ₂	NH ₃ /H ₂	
(K)							
1000	0.000	0.001	0.000	0.000	0.001	0.000	
1100	0.000	0.197	0.000	0.000	0.157	0.000	
1125	0.000	0.325	0.000	0.000	0.257	0.000	
1150	0.000	0.507	0.000	0.000	0.404	0.000	
1175	0.000	0.762	0.000	0.000	0.616	0.000	
1200	0.000	1.109	0.000	0.000	0.921	0.000	
1225	0.000	1.574	0.000	0.000	1.356	0.000	
1250	0.000	2.187	0.000	0.000	1.976	0.000	
1275	0.000	2.991	0.000	0.000	2.861	0.000	
1300	0.001	4.046	0.001	0.001	4.121	0.001	
1325	0.002	5.439	0.002	0.002	5.894	0.002	
1350	0.004	7.294	0.003	0.004	8.347	0.003	
1375	0.009	9.768	0.006	0.009	11.656	0.007	
1400	0.018	13.041	0.013	0.019	15.988	0.014	
1425	0.037	17.287	0.027	0.038	21.474	0.028	
1450	0.075	22.645	0.054	0.077	28.175	0.056	
1475	0.149	29.180	0.108	0.153	36.038	0.111	

1500	0.292	36.849	0.212	0.301	44.864	0.218
1525	0.562	45.468	0.408	0.580	54.287	0.419
1550	1.059	54.697	0.771	1.097	63.803	0.793
1575	1.953	64.052	1.426	2.029	72.824	1.469
1600	3.509	72.963	2.577	3.661	80.796	2.662
1625	6.115	80.872	4.532	6.408	87.309	4.697
1650	10.271	87.361	7.718	10.804	92.192	8.025
1675	16.485	92.239	12.635	17.374	95.527	13.170
1700	25.034	95.575	19.704	26.367	97.597	20.554
1725	35.690	97.645	29.013	37.440	98.771	30.219
1750	47.584	98.814	40.085	49.588	99.389	41.587
1775	59.451	99.422	51.894	61.461	99.699	53.537
1800	70.104	99.722	63.208	71.906	99.851	64.803
1825	78.833	99.865	73.048	80.316	99.925	74.456
1850	85.473	99.933	80.933	86.623	99.962	82.093
1875	90.244	99.966	86.856	91.106	99.980	87.768
1900	93.534	99.982	91.093	94.168	99.989	91.791
1925	95.743	99.990	94.024	96.206	99.994	94.551
1950	97.203	99.995	96.009	97.540	99.997	96.403
1975	98.159	99.997	97.335	98.404	99.998	97.629
2000	98.783	99.998	98.216	98.961	99.999	98.435
2025	99.191	99.999	98.800	99.320	100.00	98.963
2050	99.458	100.00	99.188	99.552	100.00	99.309
2075	99.634	100.00	99.447	99.701	100.00	99.536
2100	99.749	100.00	99.620	99.798	100.00	99.687
2125	99.826	100.00	99.737	99.860	100.00	99.786
2150	99.876	100.00	99.816	99.900	100.00	99.853
2175	99.909	100.00	99.871	99.925	100.00	99.898
2200	99.930	100.00	99.908	99.940	100.00	99.928
2225	99.943	100.00	99.934	99.948	100.00	99.949
2250	99.950	100.00	99.952	99.952	100.00	99.963
2275	99.954	100.00	99.965	99.954	100.00	99.973
2300	99.956	100.00	99.974	99.956	100.00	99.980
2325	99.958	100.00	99.980	99.957	100.00	99.984
2350	99.959	100.00	99.984	99.958	100.00	99.987
2375	99.960	100.00	99.987	99.959	100.00	99.989
2400	99.961	100.00	99.989	99.961	100.00	99.991
2425	99.962	100.00	99.991	99.962	100.00	99.991
2450	99.963	100.00	99.991	99.963	100.00	99.992
2475	99.964	100.00	99.992	99.963	100.00	99.992
2500	99.965	100.00	99.992	99.964	100.00	99.992

Table S14. The calculated NH₃ conversion via plasma-based NH₃ cracking at SEI = 1.2 J/cm³ and different gas temperatures (from 300 K to 900 K). The tested mixtures are 1 v/v% NH₃ in 99 v/v% N₂/H₂ mixture; 99 v/v% N₂, and 99 v/v% H₂ mixture (corresponding to Figure S9).

	Old mechanism			New mechanism			
$T_{ m g}$	NH ₃ /N ₂ /H ₂	NH ₃ /N ₂	NH ₃ /H ₂	NH ₃ /N ₂ /H ₂	NH ₃ /N ₂	NH_3/H_2	
(K)							
300	1.100	1.830	0.000	0.000	1.800	0.000	
400	2.103	2.820	-0.011	0.033	3.800	-0.013	
500	3.350	4.830	0.000	0.703	9.047	-0.001	
600	5.304	7.100	0.006	1.268	16.821	0.003	
700	7.964	16.000	0.150	2.787	35.816	0.015	
800	9.137	16.100	1.804	0.256	25.722	0.085	
900	15.701	28.300	8.757	1.173	26.580	0.000	

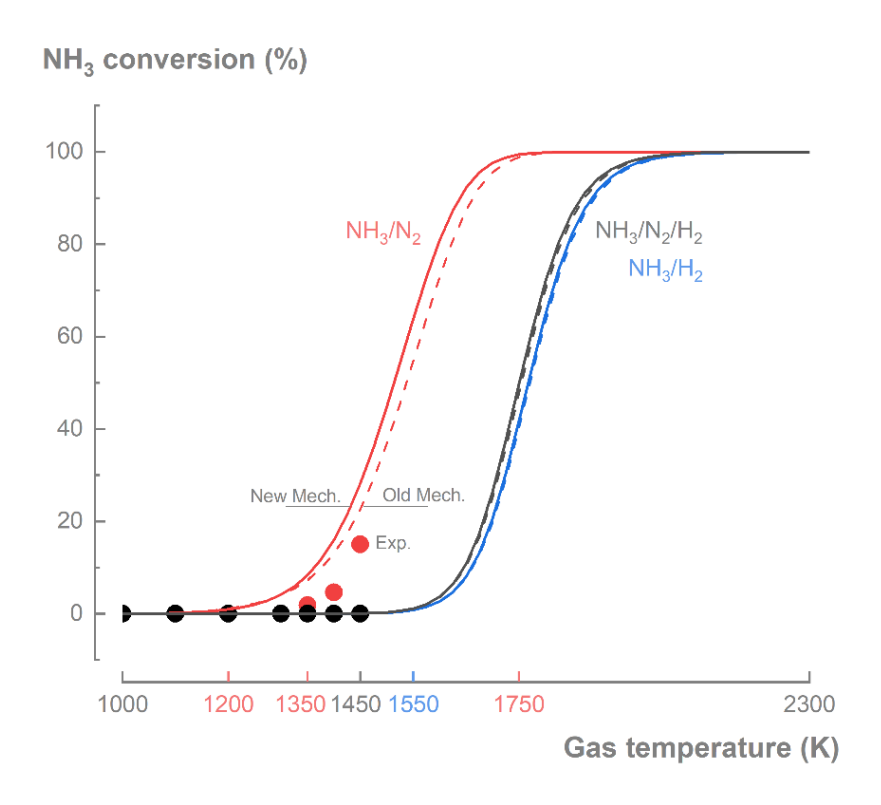


Figure S8. Calculated NH₃ conversions via thermal-based NH₃ cracking at SEI = 0 J/cm³ over a temperature range of T_g = 1000–2300 K. Solid lines represent results from the newly developed reaction mechanism, while dashed lines correspond to the previous mechanism from ⁸. Calculations are compared with experimental data (symbols). The tested mixture consisted of 1 v/v% NH₃ and (i) a 1:3 molar ratio of N₂ to H₂ (black), (ii) N₂ (red), and (iii) H₂ (blue). For detailed numerical values, see Table S13.

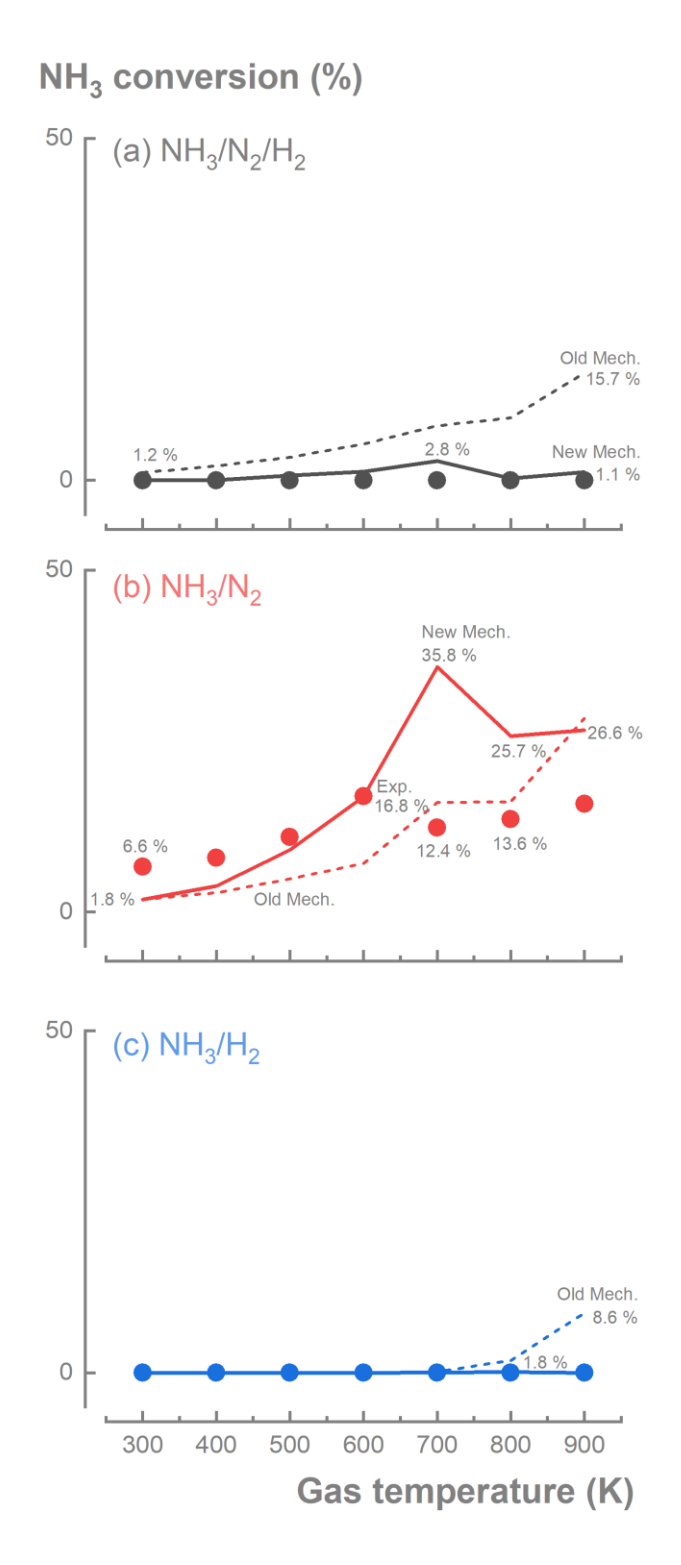


Figure S9. Calculated NH₃ conversions via plasma-based NH₃ cracking at SEI = 1.2 J/cm³ over a temperature range of T_9 = 300–900 K. Solid lines represent results from the newly developed reaction mechanism, while dashed lines correspond to the previous mechanism from ⁸. The tested mixture consisted of 1 v/v% NH₃ and (i) a 1:3 molar ratio of N₂ to H₂ (black), (ii) N₂ (red), and (iii) H₂ (blue). For detailed numerical values, see Table S14.

3. Approximation of H₂ production rate based on electron energy loss fraction

The performance of low temperature plasma-based NH₃ cracking, so basically H₂ production rate (R_{H2}), is primarly governed by by electron impact processes, as is clearly shown in Figure 1 in the main manuscript:

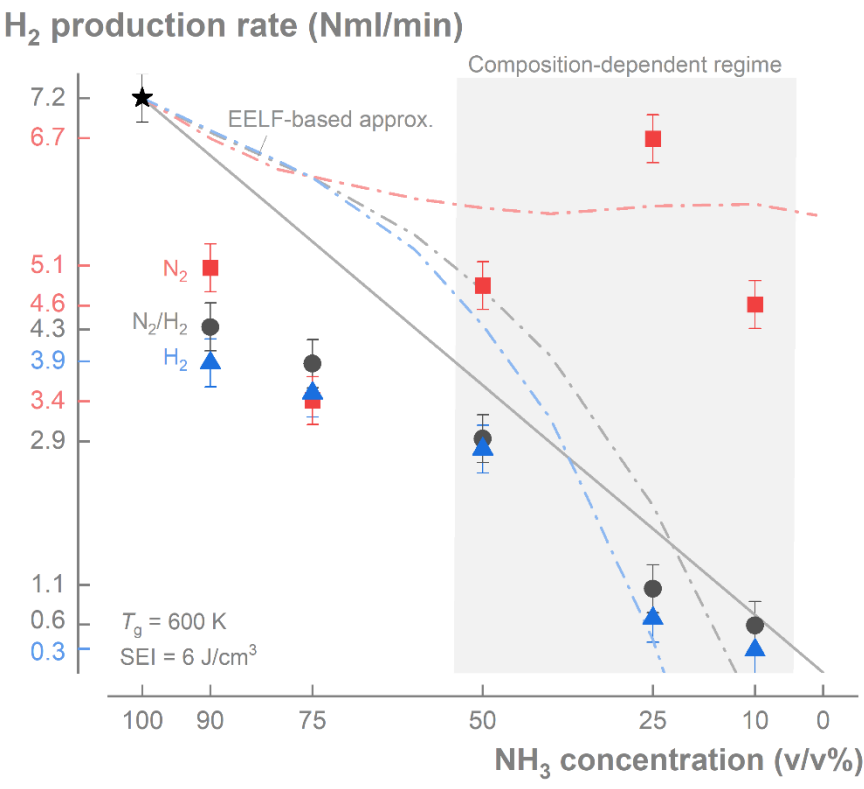


Figure S10. Reprinted from the main manuscript (Figure 1). The measured H₂ production rate generally decreases as the initial NH₃ concentration is lowered. Initially, the three mixtures behave similarly up to the composition-dependent regime. In this regime, the H₂ production rate for NH₃/H₂ and NH₃/N₂/H₂ (fixed N₂:H₂ ratio of 1:3) continues to decline, whereas that for NH₃/N₂ recovers. A linear dilution approximation (solid line) indicates which mixtures have a positive or negative contribution, whereas an electron energy loss fraction (EELF)-based approximation (dash-dotted line) succeeds in capturing the differences between the mixtures.

In this section, we describe the approxiation method based on electron energy loss fraction calculated using BOLSIG+ ²⁶ in combination with cross section data for NH₃, N₂, and H₂ (see Table S15 for references).

For a gas temperature $T_g = 600 \text{ K}$ and various NH₃ concentration (100 v/v% to 1 v/v%), the electron energy loss fraction for each specie (Figure S11) and for the key electron impact processes (Figure S12) are calculated. In this study, the three important electron impact processes that were identified based on

the chemical analysis (Section S4) are: (i) electron impact dissociation of NH₃, (ii) electron impact electronic excitation of N₂, and (iii) electron impact dissociation of H₂. The dissociation of NH₃ via electron impact (reactions RS48–RS55 in Table S15) directly contributes to increased NH₃ conversion. Meanwhile, electronic excitations of N₂ (RS18–RS25) produce metastable species such as N₂(A³) and N₂(a¹) upon relaxation, which subsequently promote NH₃ conversion through Penning dissociation (RS114 and RS115). In contrast, H₂ dissociation via electron impact (RS34–RS42) has a negative effect on NH₃ conversion, primarily by enhancing NH₂ radical recombination (RS78a and RS80). The energy loss fractions are calculated at *E/N* conditions observed in the experiments (see Figures S3a).

By using the electron energy loss fractions (EELF) associated with key electron impact processes—specifically, NH₃ dissociation, N₂ electronic excitation, and H₂ dissociation—we can define an approximation factor (σ). This factor represents the net EELF contribution to NH₃ dissociation and N₂ excitation, minus the EELF associated with H₂ dissociation. The result is then normalized to the value obtained at 100 v/v% NH₃. In essence, σ quantifies the relative influence of competing electron-driven processes on NH₃ conversion, using pure NH₃ as a reference point. A higher or lower σ value indicates how the presence of other gases (e.g., H₂ or N₂) modulates the efficiency of NH₃-related reactions by altering the distribution of electron energy losses:

$$\alpha = \frac{\left(ELF_{NH_3.dissociation} + ELF_{N_2.electronic} - ELF_{H_2.dissociation}\right)}{\left(ELF_{NH_3.dissociation} + ELF_{N_2.electronic} - ELF_{H_2.dissociation}\right)_{@100v/v\%NH_3}}$$
(S1)

The approximated H_2 production is in turn obtained by multiplying a reference H_2 production rate, achieved at 100 v/v% NH₃ concentration, by this approximation factor. The calculated results are displayed dashed-dotted lines in Figure 1 in the main manuscript (see above).

$$R_{H_2.approximated} [Nml/min] = R_{H_2@100v/v\%NH_3} \times \alpha$$
 (S2)

This approximation strongly supports that the variation in energy consumed by different electron impact reactions play a pivotal role in plasma-based NH₃ cracking.

Electron energy loss fraction to each specie

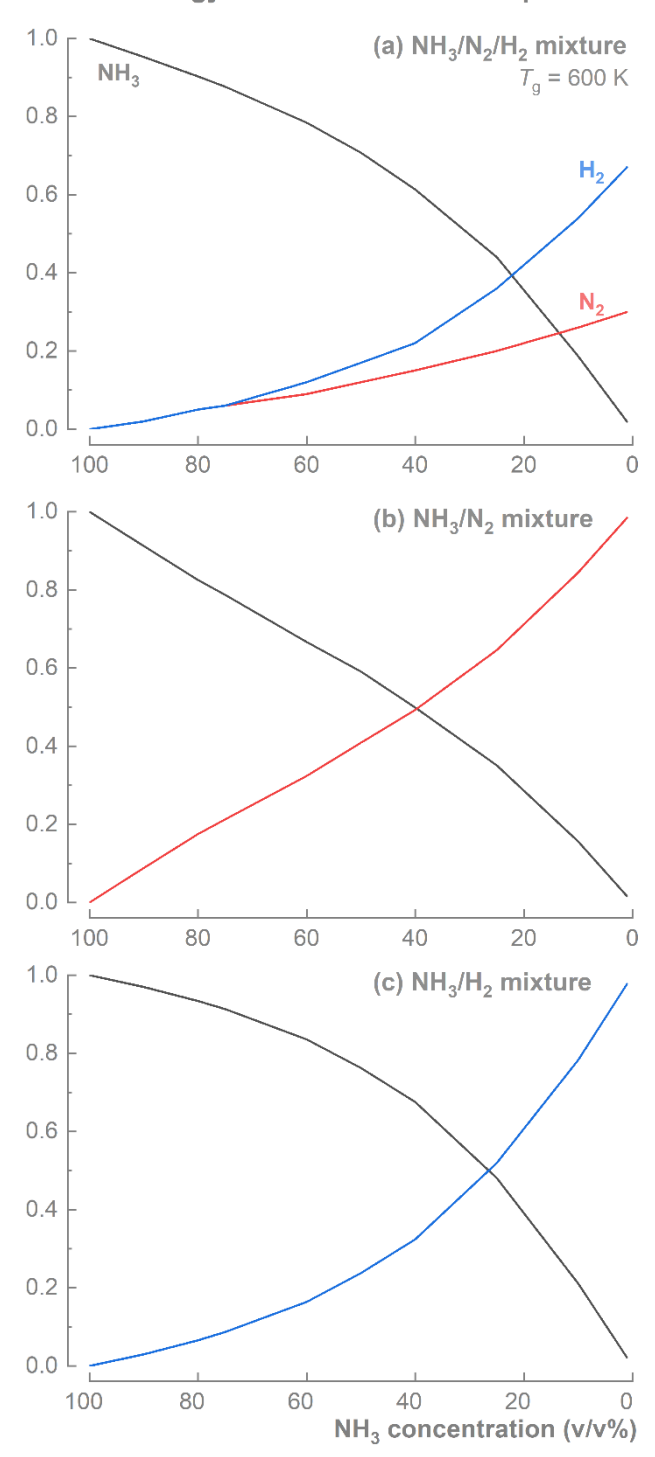
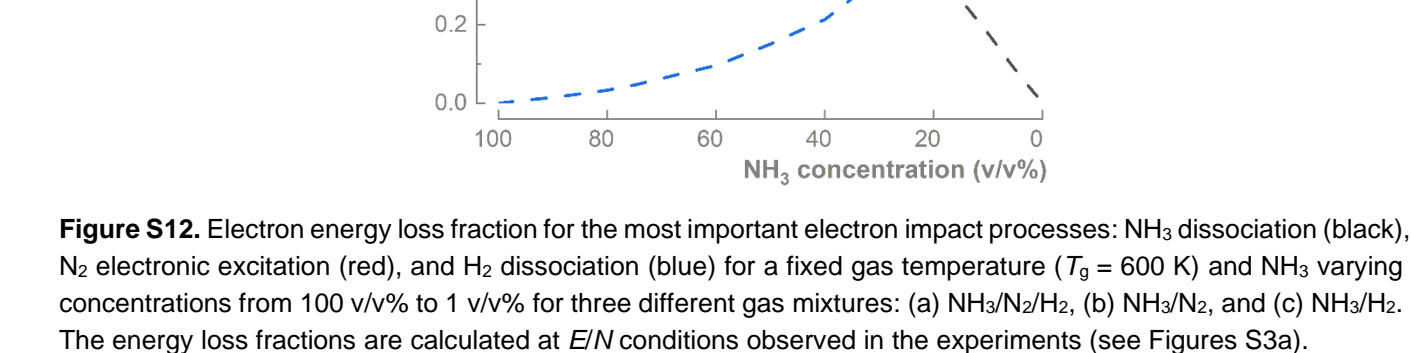


Figure S11. Electron energy loss fraction to each specie: NH₃ (black), N₂ (red), and H₂ (blue) for a fixed gas temperature ($T_g = 600 \text{ K}$) and varying NH₃ concentrations from 100 v/v% to 1 v/v% for three different gas mixtures: (a) NH₃/N₂/H₂, (b) NH₃/N₂, and (c) NH₃/H₂. The energy loss fractions are calculated at E/N conditions observed in the experiments (see Figures S3a).

Electron energy loss fraction

to important processes 1.0 (a) NH₃/N₂/H₂ mixture $T_{\rm q} = 600 \, {\rm K}$ NH₃ dissociation 0.8 0.6 0.4 H₂ dissociation 0.2 N₂ electronic excitation 0.0 60 40 20 1.0 (b) NH₃/N₂ mixture 0.8 0.6 0.4 0.2



0.0

1.0

0.8

0.6

0.4

100

80

60

40

20

(c) NH₃/H₂ mixture

4. Extended chemical analysis

4.1. Production and consumption of the main species

Figure S13 and S14 illustrate the total production and loss of the different species (except vibrationally excited species and excited H₂ in singlet state). These values are obtained by integrating the instantaneous production and loss rates of the contributing reactions over the entire duration of the simulation (which reflects the experimental residence time). Thus, the overall production and loss have a unit of number of species (molecule) per cm³. In addition, Figure S15 demonstrates the net productions (net changes), where the negative and positive values indicate loss and production, respectively.

Total production (10¹⁶ molecule/cm³)

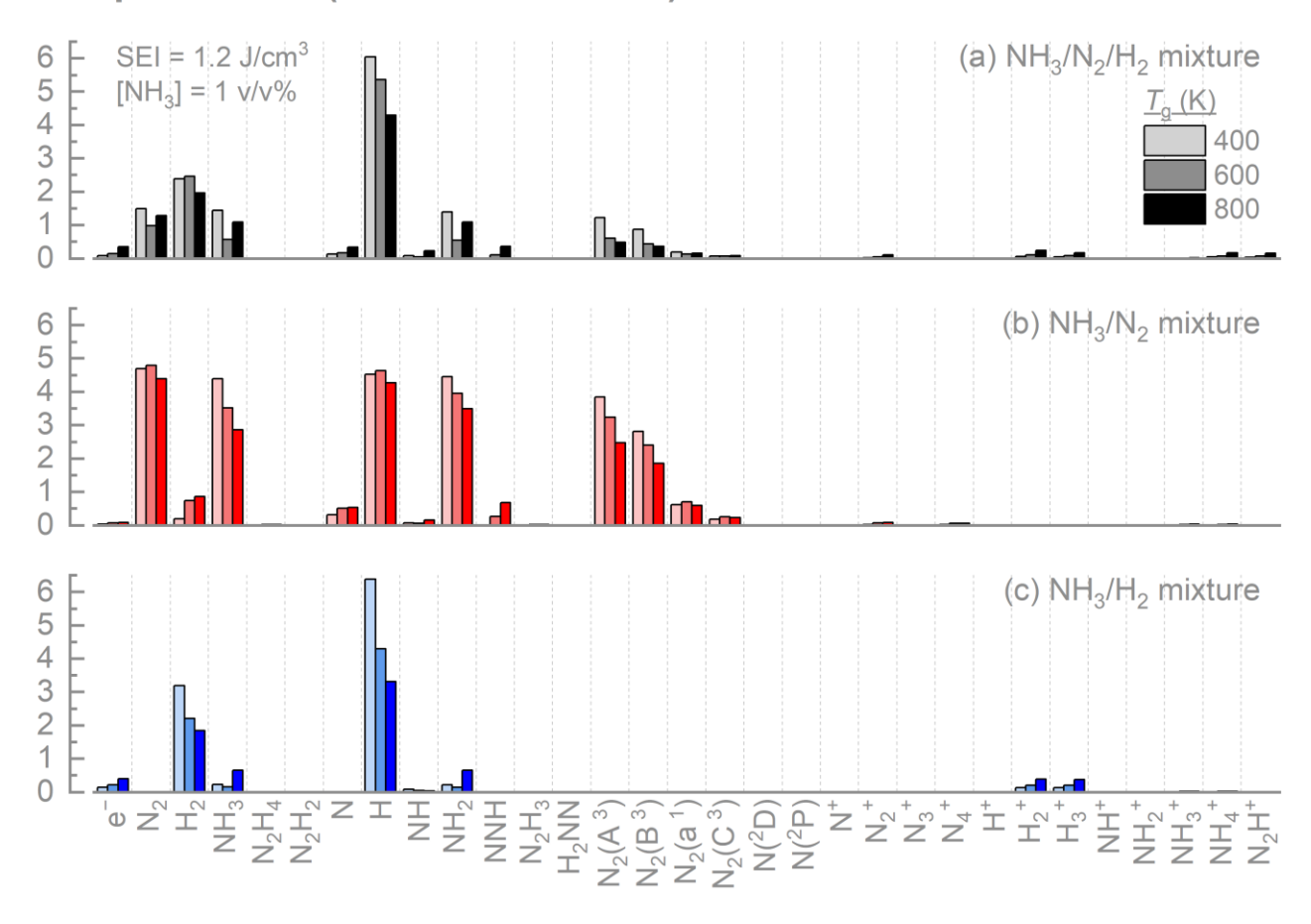


Figure S13. Total production for the main species in 1 v/v% NH₃ with (a) a 1:3 molar ratio of N₂/H₂, (b) N₂, and (c) H₂ for three different $T_g = 400$, 600, and 800 K (from left to right). The specific energy input is 1.2 J/cm³ (corresponding to 20 W at 1 SLPM of the total flow rate) and E/N used in analysis are equal to the values in Table S12.

Total loss (10¹⁶ molecule/cm³)

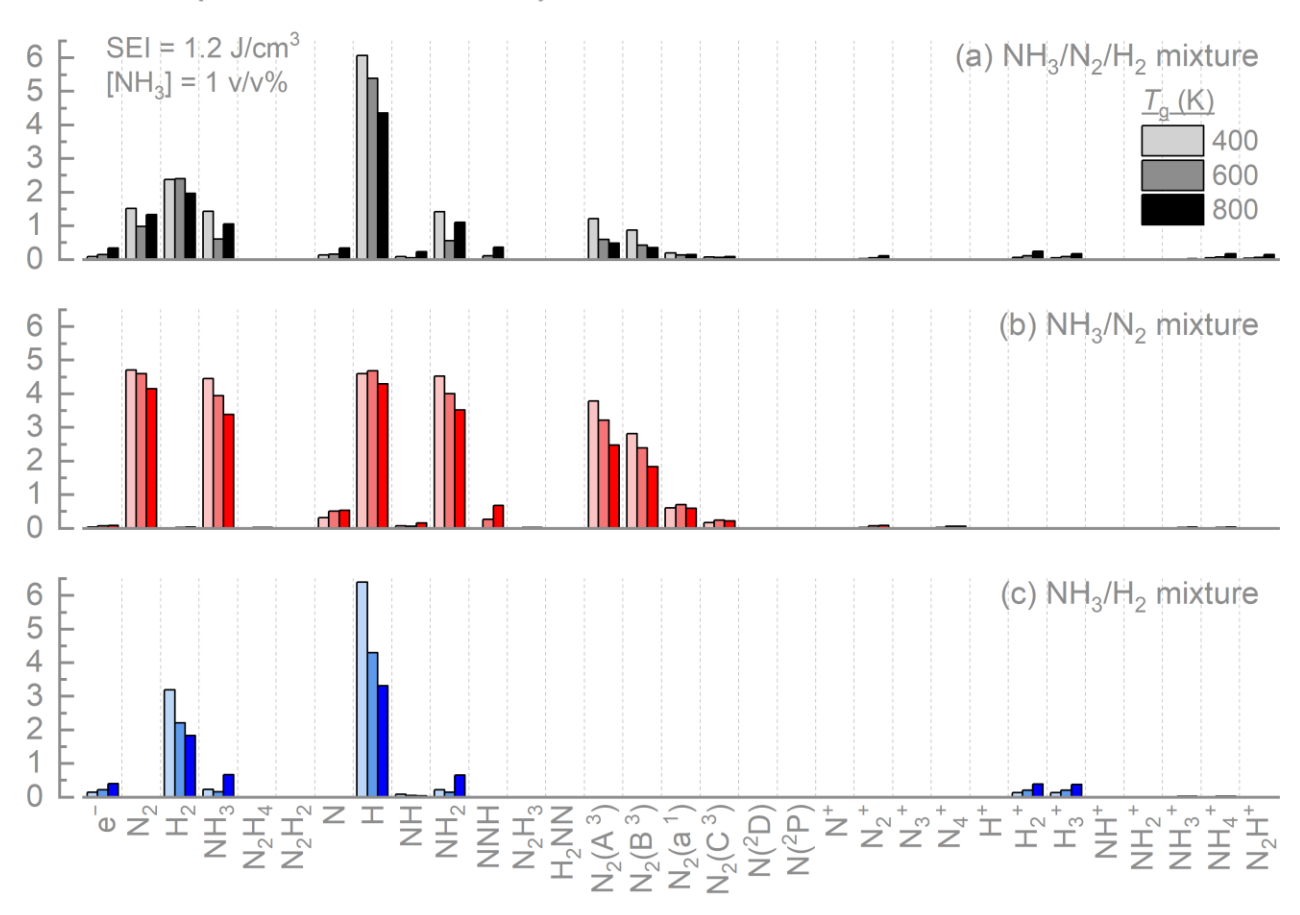


Figure S14. Total loss (consumption) for the main species in 1 v/v% NH₃ with (a) a 1:3 molar ratio of N₂/H₂, (b) N₂, and (c) H₂ for three different $T_g = 400$, 600, and 800 K (from left to right). The specific energy input is 1.2 J/cm³ (corresponding to 20 W at 1 SLPM of the total flow rate) and E/N used in analysis are equal to the values in Table S12.



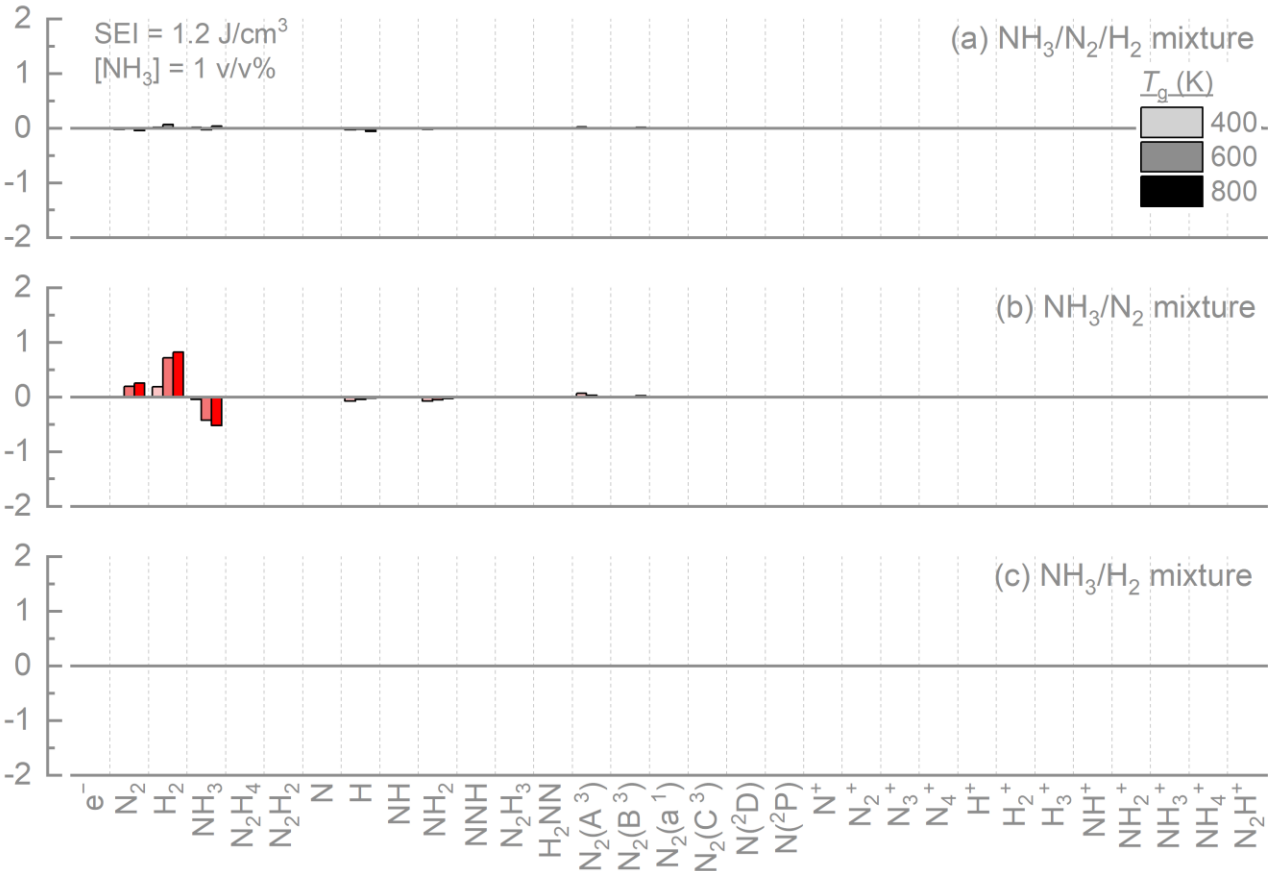


Figure S15. Net production for the main species in 1 v/v% NH₃ with (a) a 1:3 molar ratio of N₂/H₂, (b) N₂, and (c) H₂ for three different $T_g = 400$, 600, and 800 K (from left to right). The specific energy input is 1.2 J/cm³ (corresponding to 20 W at 1 SLPM of the total flow rate) and E/N used in analysis are equal to the values in Table S12.

4.2. Reaction rates and contributions of the main elementary reactions

We identified elementary reactions by investigating the main species and their rates of production and loss. As a result, a total of 26 reactions are identified as elementary reactions, each exhibiting integrated rates exceeding 10¹⁵ molecule/cm³. Figure S16 shows the overall contribution of each reaction (which is the reaction rate integrated over the entire duration of the simulation) for three mixture conditions and three gas temperature conditions.

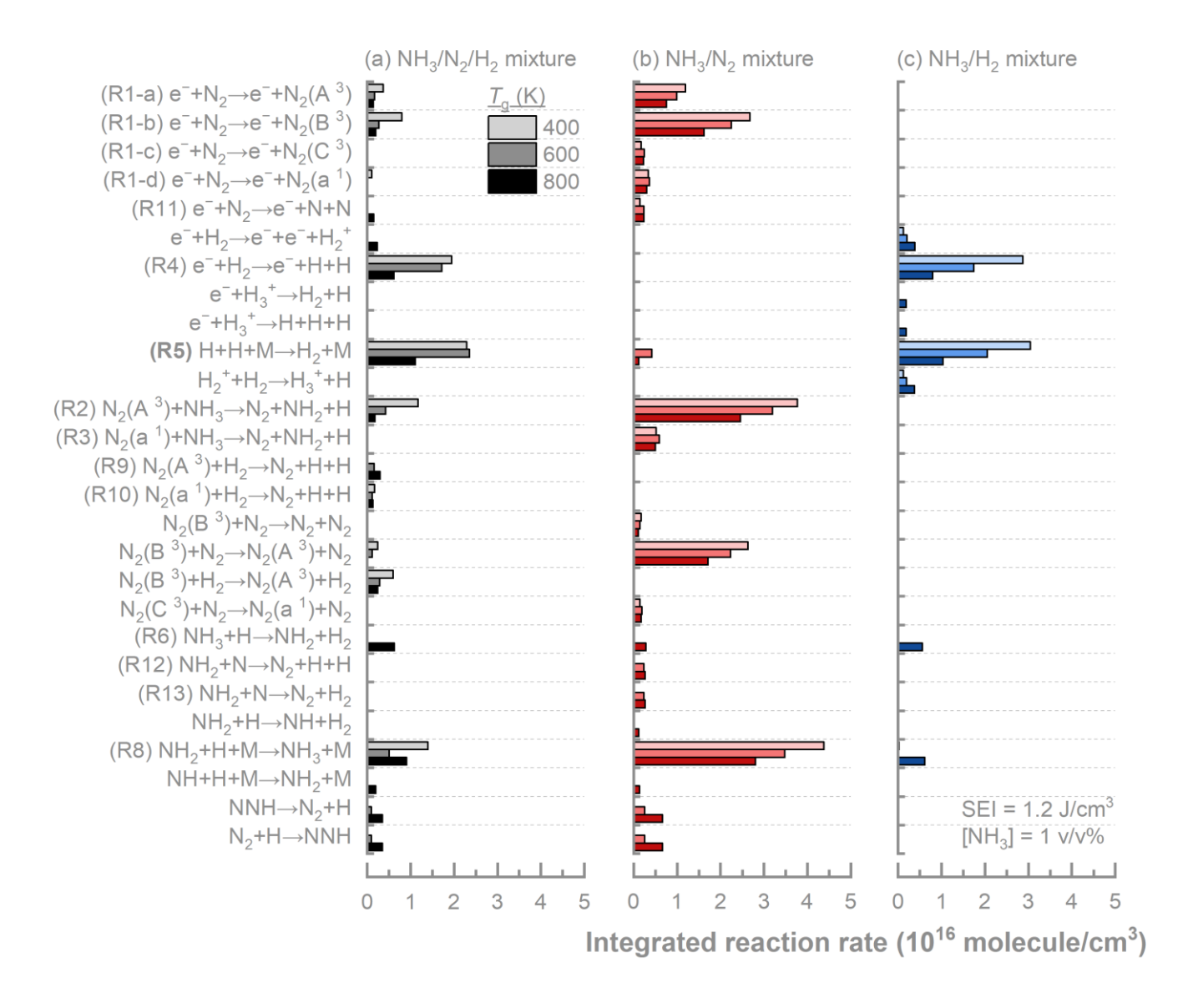


Figure S16. Overview of the overall contribution of the main elementary reactions in 1 v/v% NH₃ with (a) a 1:3 molar ratio of N₂/H₂, (b) N₂, and (c) H₂ for three different $T_g = 400$, 600, and 800 K (from top to bottom). The specific energy input is 1.2 J/cm³ (corresponding to 20 W at 1 SLPM of the total flow rate) and E/N used in analysis are equal to the values in Table S12.

To better understand the chemical mechanism, we depict the detailed contributions of the elementary reactions to both production and loss of the main species for the decomposition of NH₃ (Figure S17 to Figure S27): N_2 , N_2 (A 3), N_2 (B 3), N_2 (C 3), N_2 (a 1), N, NH₃, NH₂, NH, H, H₂.

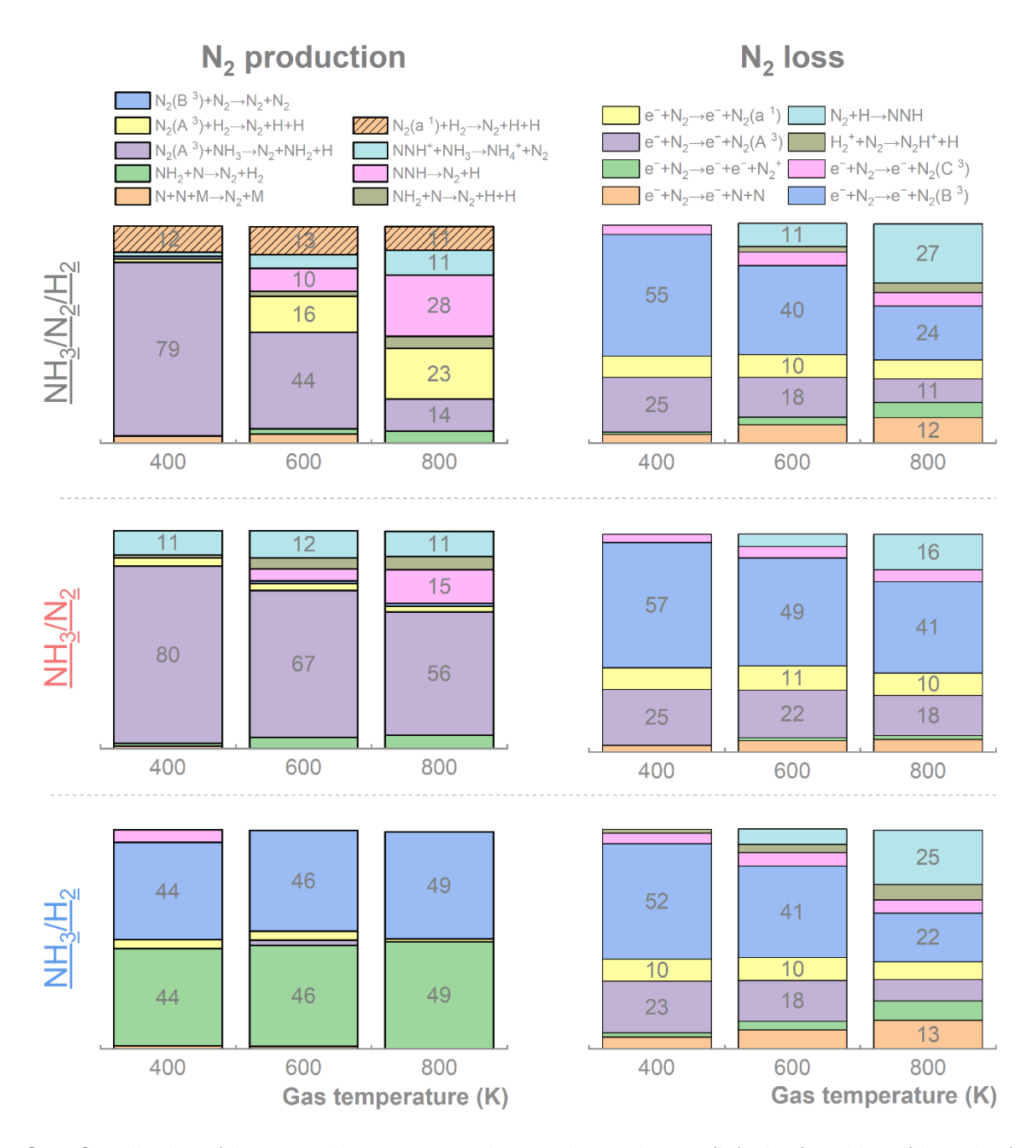


Figure S17. Contribution of the main elementary reactions to the production (left plots) and loss (right plots) of N_2 in a 1 v/v% NH_3 mixture with different balance gases: a 1:3 molar ratio of N_2/H_2 (top row), N_2 (middle row), and H_2 (bottom row). Within each plot, results are shown from left to right for three gas temperatures, $T_g = 400$, 600, and 800 K. The specific energy input is 1.2 J/cm³, corresponding to 20 W at a total flow rate of 1 SLPM. The E/N values used for the analysis are listed in Table S12.



Figure S18. Contribution of main elementary reactions to the production (left plots) and loss (right plots) of $N_2(A^3)$ in a 1 v/v% NH_3 mixture with different balance gases: a 1:3 molar ratio of N_2/H_2 (top row), N_2 (middle row), and H_2 (bottom row). Within each plot, results are shown from left to right for three gas temperatures, $T_g = 400$, 600, and 800 K. The specific energy input is 1.2 J/cm³, corresponding to 20 W at a total flow rate of 1 SLPM. The E/N values used for the analysis are listed in Table S12.

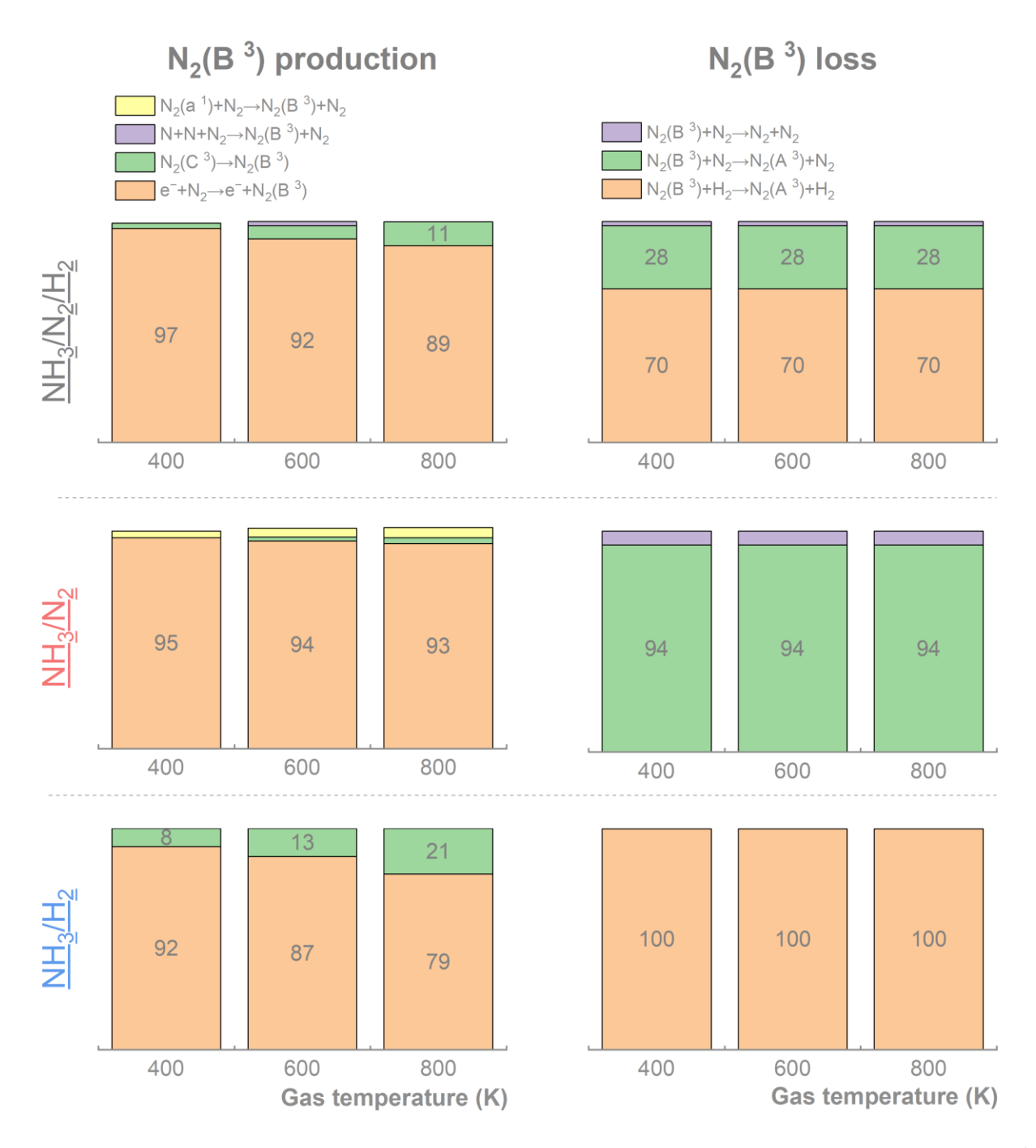


Figure S19. Contribution of main elementary reactions to the production (left plots) and loss (right plots) of $N_2(B^3)$ in a 1 v/v% NH₃ mixture with different balance gases: a 1:3 molar ratio of N_2/H_2 (top row), N_2 (middle row), and H_2 (bottom row). Within each plot, results are shown from left to right for three gas temperatures, $T_g = 400$, 600, and 800 K. The specific energy input is 1.2 J/cm³, corresponding to 20 W at a total flow rate of 1 SLPM. The E/N values used for the analysis are listed in Table S12.



Figure S20. Contribution of main elementary reactions to the production (left plots) and loss (right plots) of $N_2(C^3)$ in a 1 v/v% NH₃ mixture with different balance gases: a 1:3 molar ratio of N_2/H_2 (top row), N_2 (middle row), and H_2 (bottom row). Within each plot, results are shown from left to right for three gas temperatures, $T_g = 400$, 600, and 800 K. The specific energy input is 1.2 J/cm³, corresponding to 20 W at a total flow rate of 1 SLPM. The E/N values used for the analysis are listed in Table S12.

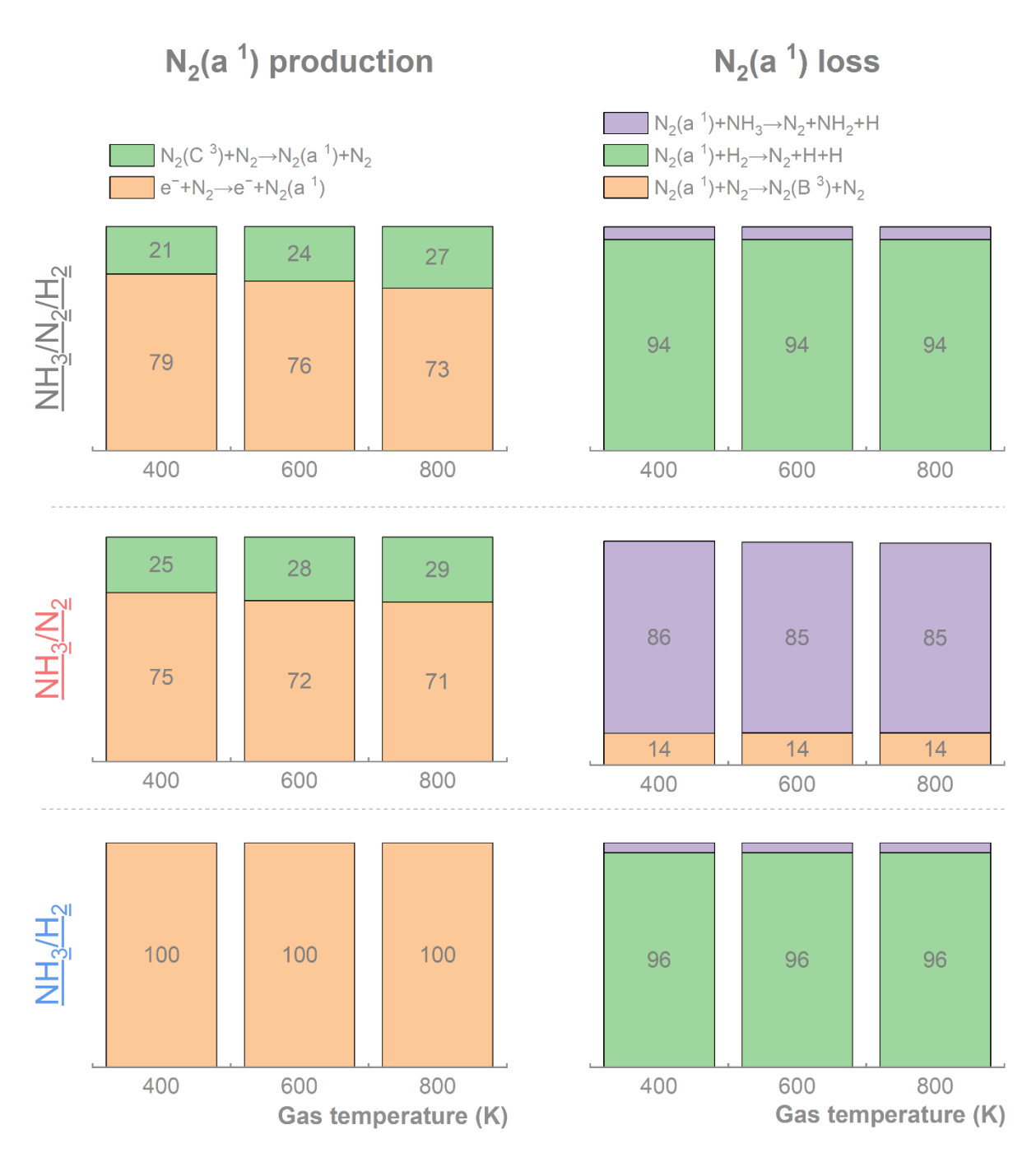


Figure S21. Contribution of main elementary reactions to the production (left plots) and loss (right plots) of N₂(a ¹) in a 1 v/v% NH₃ mixture with different balance gases: a 1:3 molar ratio of N₂/H₂ (top row), N₂ (middle row), and H₂ (bottom row). Within each plot, results are shown from left to right for three gas temperatures, $T_g = 400$, 600, and 800 K. The specific energy input is 1.2 J/cm³, corresponding to 20 W at a total flow rate of 1 SLPM. The *E/N* values used for the analysis are listed in Table S12.

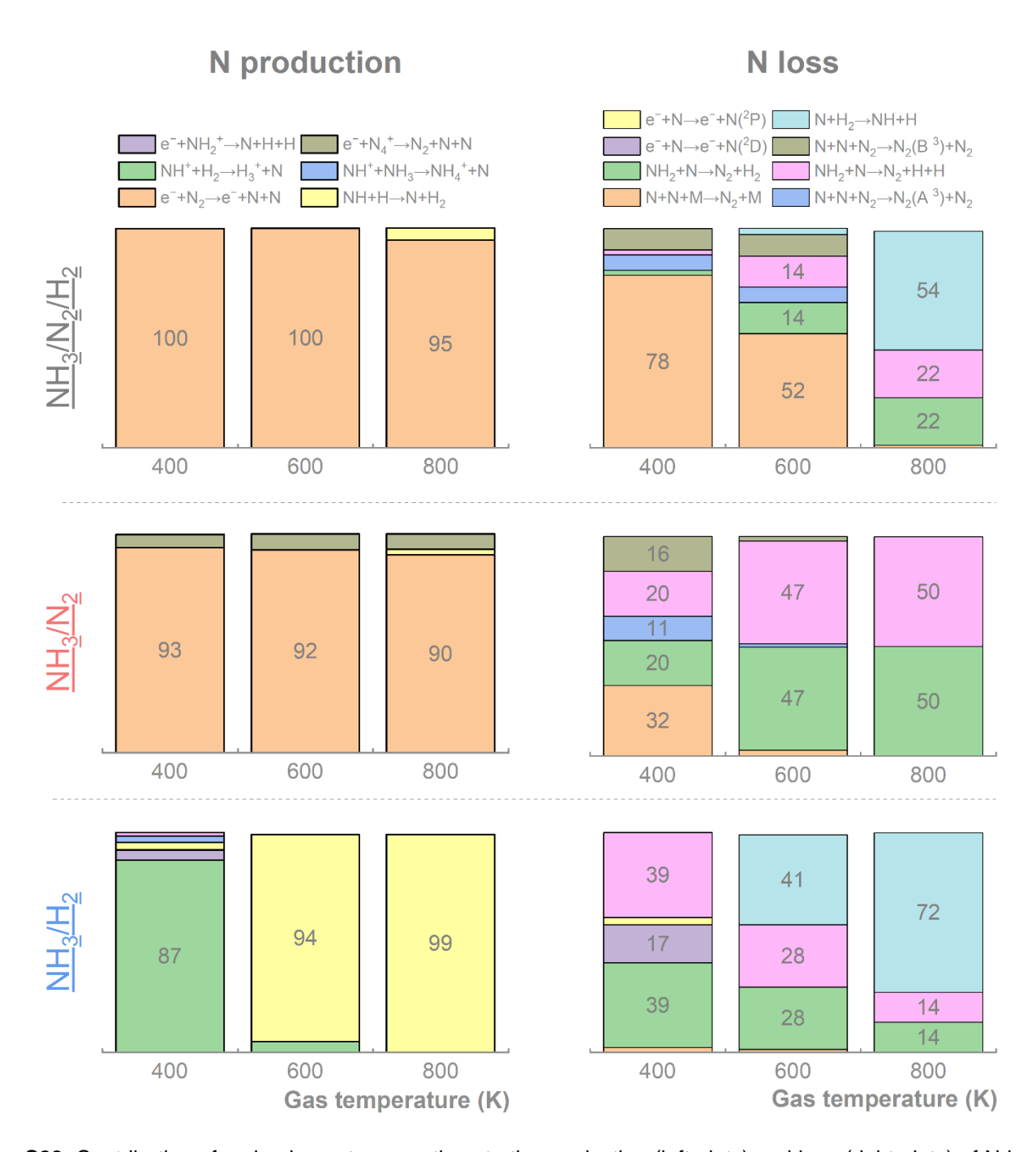


Figure S22. Contribution of main elementary reactions to the production (left plots) and loss (right plots) of N in a 1 v/v% NH₃ mixture with different balance gases: a 1:3 molar ratio of N₂/H₂ (top row), N₂ (middle row), and H₂ (bottom row). Within each plot, results are shown from left to right for three gas temperatures, $T_g = 400$, 600, and 800 K. The specific energy input is 1.2 J/cm³, corresponding to 20 W at a total flow rate of 1 SLPM. The E/N values used for the analysis are listed in Table S12.

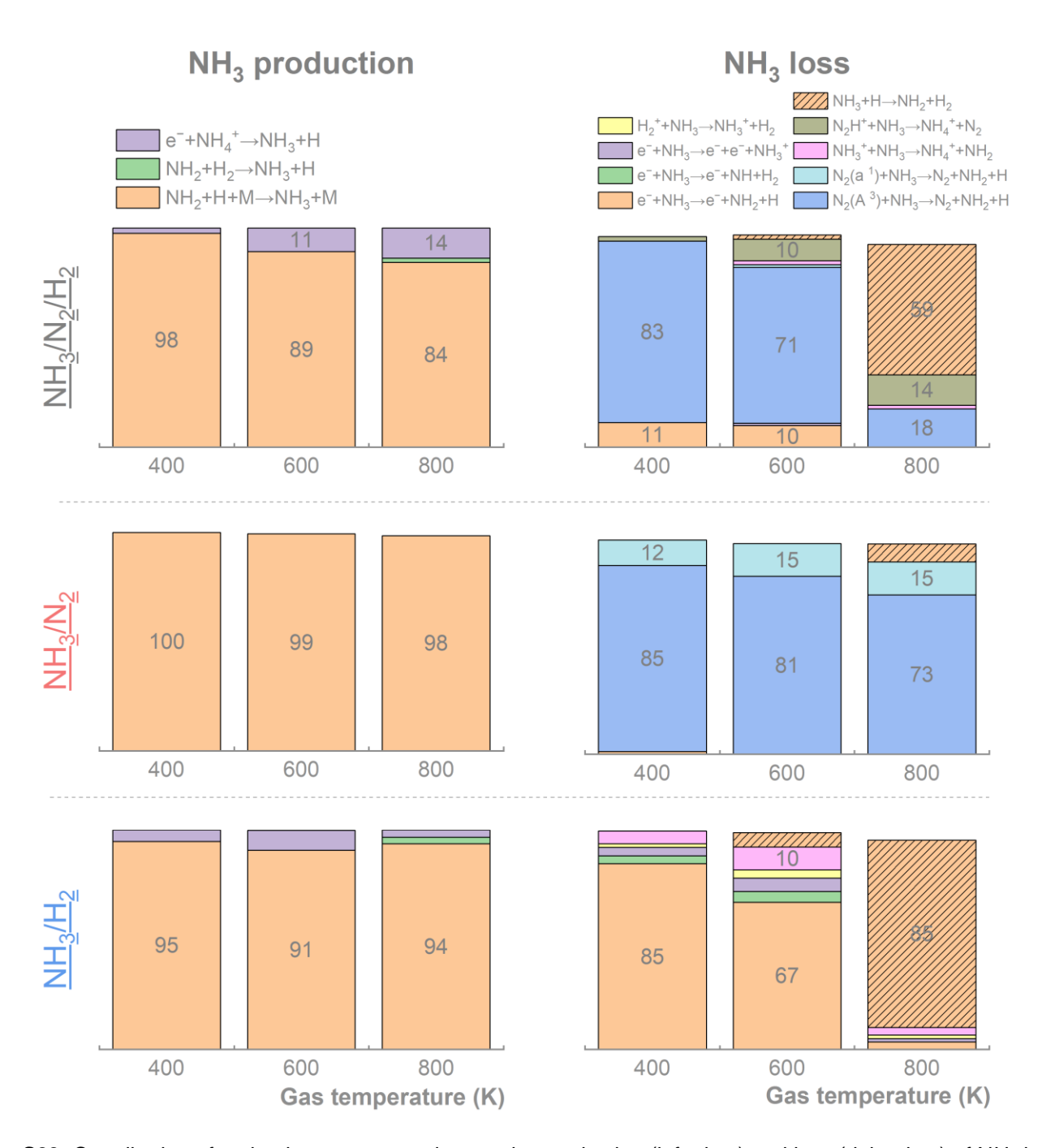


Figure S23. Contribution of main elementary reactions to the production (left plots) and loss (right plots) of NH₃ in a 1 v/v% NH₃ mixture with different balance gases: a 1:3 molar ratio of N₂/H₂ (top row), N₂ (middle row), and H₂ (bottom row). Within each plot, results are shown from left to right for three gas temperatures, $T_g = 400$, 600, and 800 K. The specific energy input is 1.2 J/cm³, corresponding to 20 W at a total flow rate of 1 SLPM. The E/N values used for the analysis are listed in Table S12.

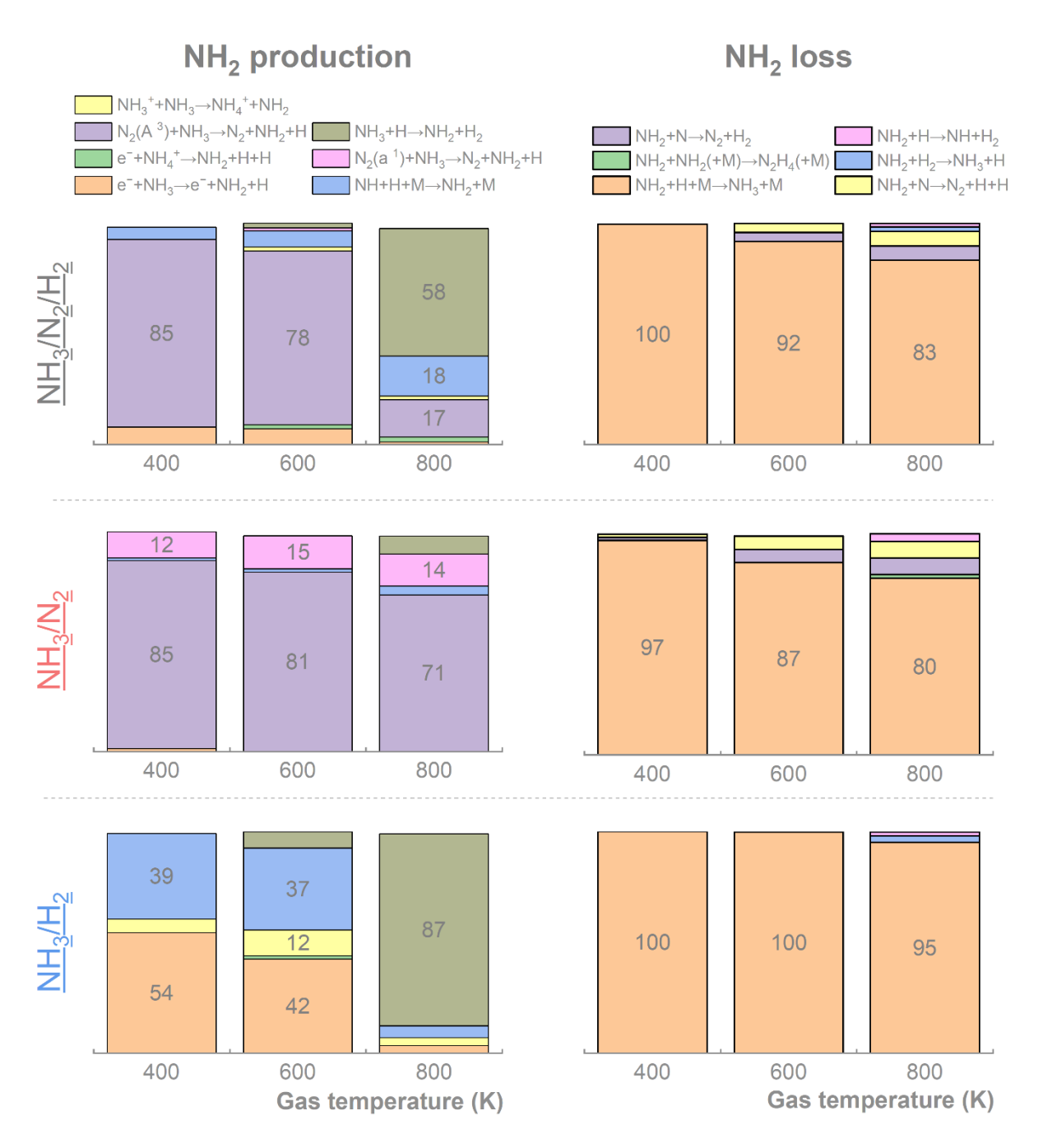


Figure S24. Contribution of main elementary reactions to the production (left plots) and loss (right plots) of NH₂ in a 1 v/v% NH₃ mixture with different balance gases: a 1:3 molar ratio of N₂/H₂ (top row), N₂ (middle row), and H₂ (bottom row). Within each plot, results are shown from left to right for three gas temperatures, $T_g = 400$, 600, and 800 K. The specific energy input is 1.2 J/cm³, corresponding to 20 W at a total flow rate of 1 SLPM. The E/N values used for the analysis are listed in Table S12.

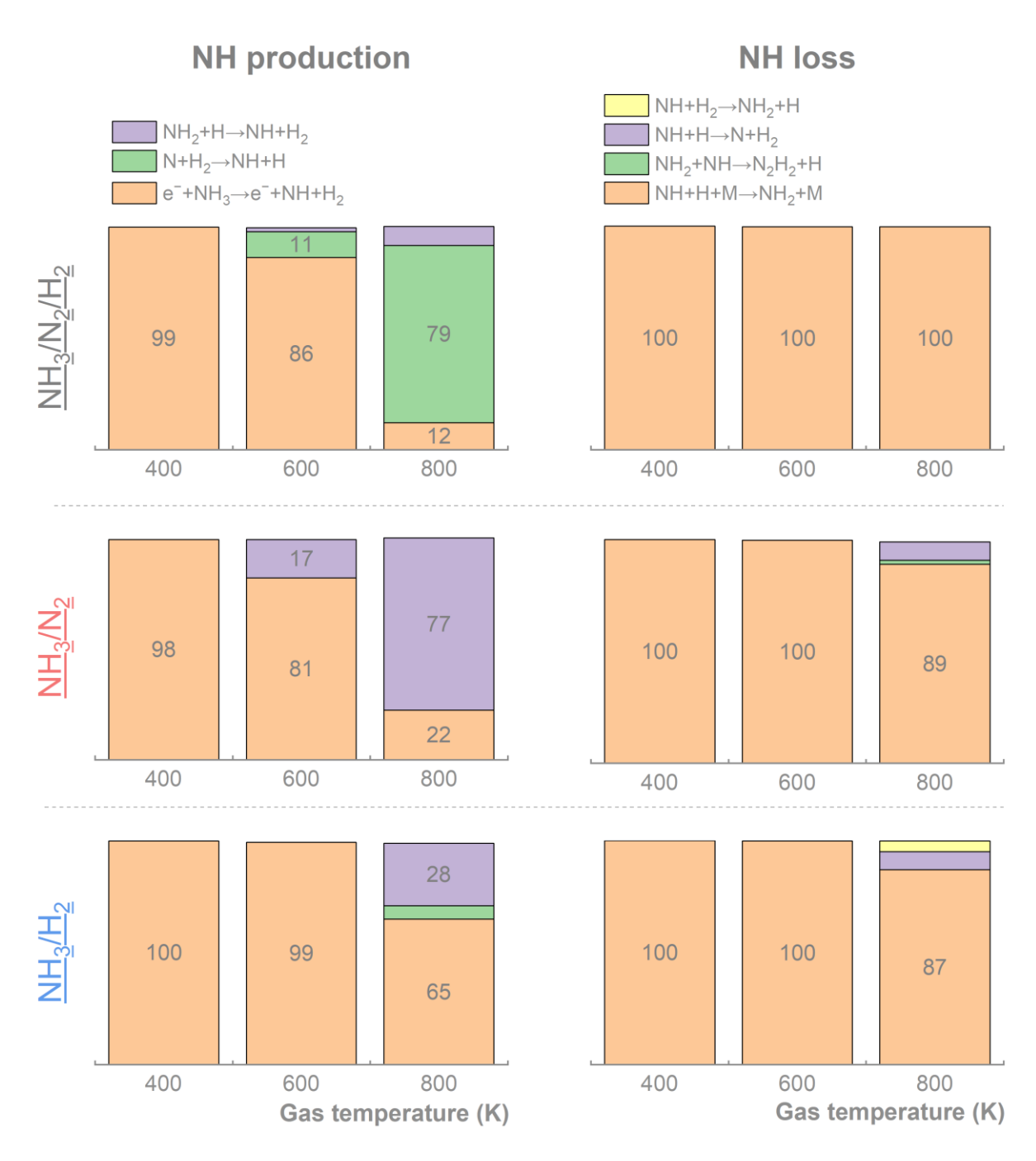


Figure S25. Contribution of main elementary reactions to the production (left plots) and loss (right plots) of NH in a 1 v/v% NH₃ mixture with different balance gases: a 1:3 molar ratio of N_2/H_2 (top row), N_2 (middle row), and H_2 (bottom row). Within each plot, results are shown from left to right for three gas temperatures, $T_g = 400$, 600, and 800 K. The specific energy input is 1.2 J/cm³, corresponding to 20 W at a total flow rate of 1 SLPM. The E/N values used for the analysis are listed in Table S12.

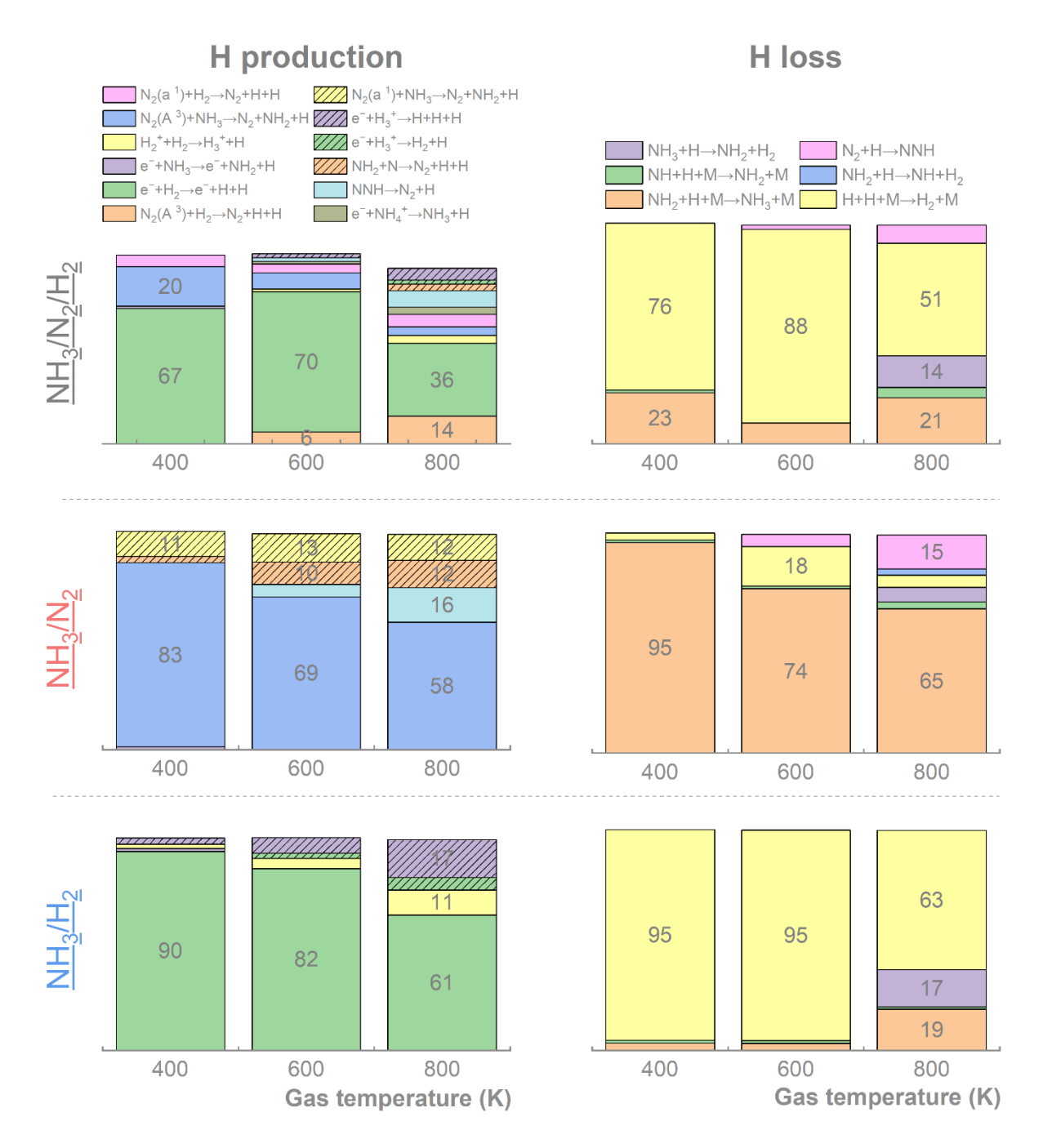


Figure S26. Contribution of main elementary reactions to the production (left plots) and loss (right plots) of H in a 1 v/v% NH₃ mixture with different balance gases: a 1:3 molar ratio of N₂/H₂ (top row), N₂ (middle row), and H₂ (bottom row). Within each plot, results are shown from left to right for three gas temperatures, $T_g = 400$, 600, and 800 K. The specific energy input is 1.2 J/cm³, corresponding to 20 W at a total flow rate of 1 SLPM. The E/N values used for the analysis are listed in Table S12.

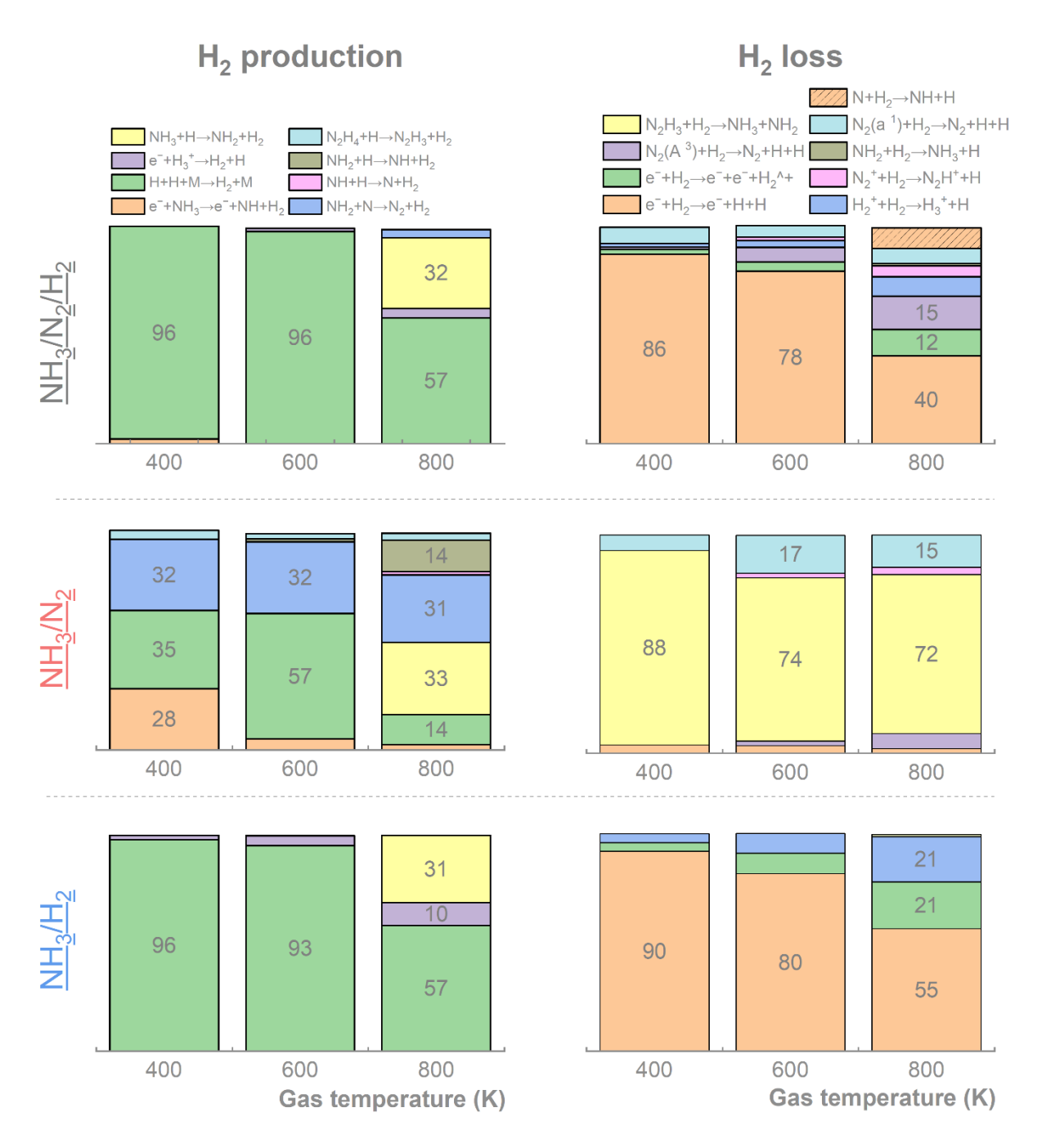


Figure S27. Contribution of main elementary reactions to the production (left plots) and loss (right plots) of H_2 in a 1 v/v% NH_3 mixture with different balance gases: a 1:3 molar ratio of N_2/H_2 (top row), N_2 (middle row), and H_2 (bottom row). Within each plot, results are shown from left to right for three gas temperatures, $T_g = 400$, 600, and 800 K. The specific energy input is 1.2 J/cm³, corresponding to 20 W at a total flow rate of 1 SLPM. The E/N values used for the analysis are listed in Table S12.

4.3. The difference between $N_2(B^3)$ and $N_2(A^3)$

Although $N_2(A^3)$ has a lower threshold energy (6.73 eV compared to ~7.7 eV of $N_2(B^3)$), our analysis shows that the dominant pathway for $N_2(A^3)$ production is quenching of $N_2(B^3)$ to $N_2(A^3)$ (Figure S18). This behavior can be attributed to (i) the larger cross section for electron-impact excitation to $N_2(B^3)$, which leads to higher rate coefficients compared to direct excitation to $N_2(A^3)$ (Figure S28); and (ii) the fast quenching rates of $N_2(B^3)$ to $N_2(A^3)$.

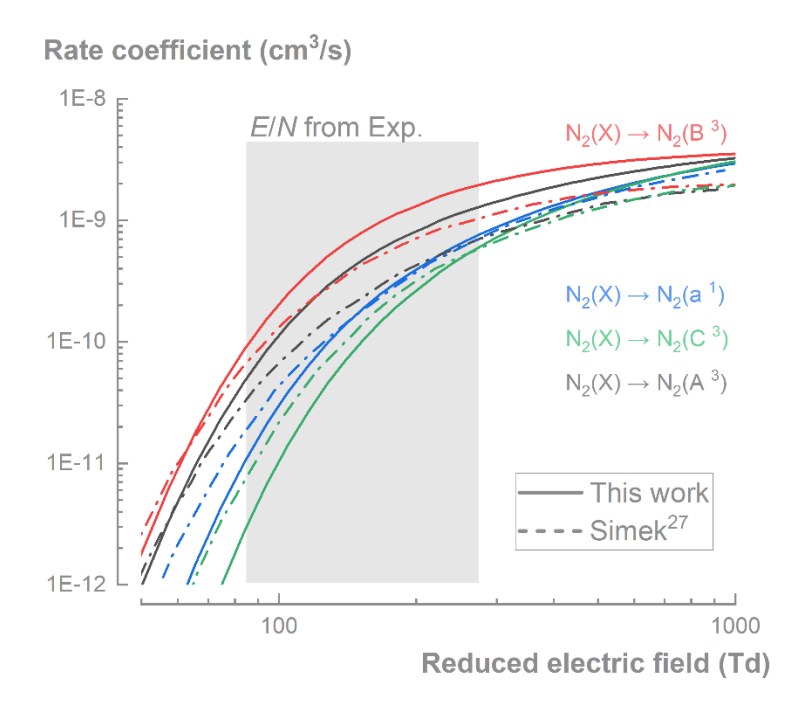


Figure S28. Reaction rate coefficients for electron-impact excitations: $N_2(X) \rightarrow N_2(A^3)$ (black), $N_2(X) \rightarrow N_2(B^3)$ (red), $N_2(X) \rightarrow N_2(C^3)$ (green), and $N_2(X) \rightarrow N_2(a^1)$ (blue). Solid lines represent the present study, while dot-dashed lines indicate data from Simek²⁷. Across a wide range of E/N, the excitation to $N_2(B^3)$ exhibits consistently higher rate coefficients than the other transitions, supporting the conclusion that $N_2(B^3)$ is the main contributor to $N_2(A^3)$ production.

Although the reaction rate coefficient for $N_2(B^3)$ is higher than that for $N_2(A^3)$, leading to greater production of $N_2(B^3)$, its (non-dissociative) quenching by N_2 to form $N_2(A^3)$ is at least an order of magnitude faster than its dissociative quenching (Penning dissociation) with NH₃ (Figure S29). Consequently, abundant $N_2(B^3)$ yields only $N_2(A^3)$, without contributing to Penning dissociation that produces NH₂ and H radicals. In contrast, quenching of $N_2(A^3)$ by N_2 to the ground state is four orders of magnitude slower than Penning dissociation of NH₃ by $N_2(A^3)$ (Figure S29). Therefore, Penning

dissociation of NH₃ by $N_2(A^3)$ plays a dominant role in N_2 -enriched gas compositions, while Penning dissociation of NH₃ by $N_2(B^3)$ does not.

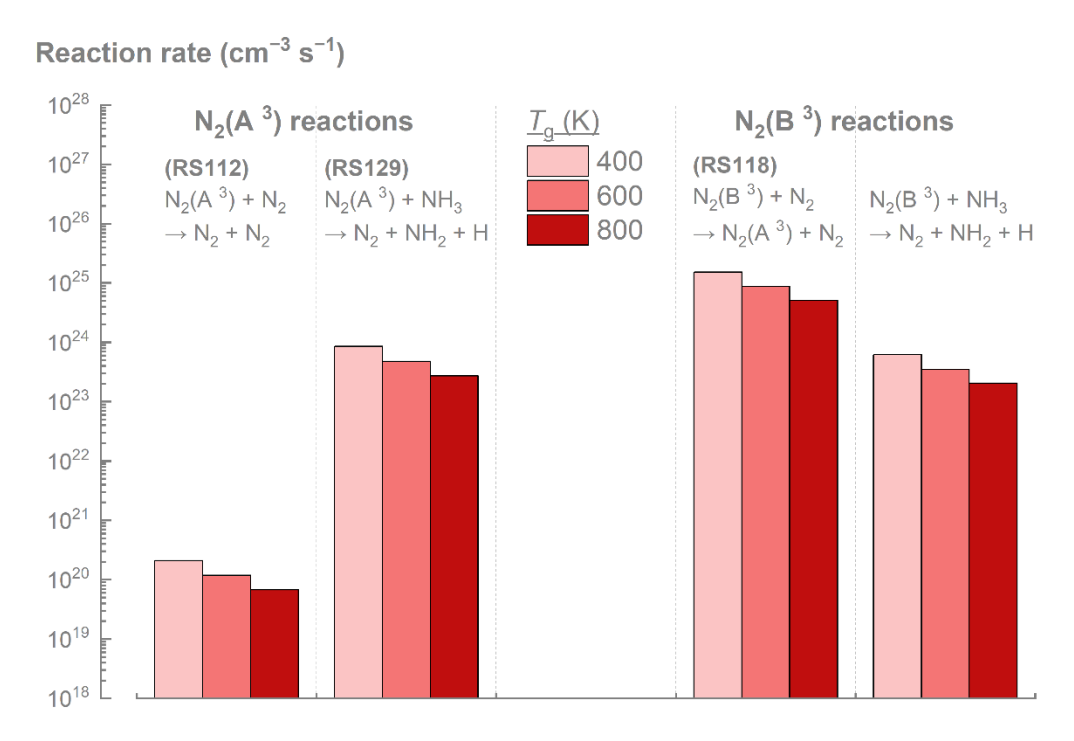


Figure S29. Comparison of reaction rates for four quenching processes of $N_2(A^3)$ and $N_2(B^3)$. Two involve quenching by N_2 to lower excited states, and two involve Penning dissociation of NH_3 : (i) $N_2(A^3) + N_2 \rightarrow N_2 + N_2$; (ii) $N_2(A^3) + NH_3 \rightarrow N_2 + NH_2 + H$; (iii) $N_2(B^3) + N_2 \rightarrow N_2(A^3) + N_2$; and (iv) $N_2(B^3) + NH_3 \rightarrow N_2 + NH_2 + H$. Reaction rates were obtained by multiplying the rate coefficients (RS112, RS118, RS129 in Table S15) by the estimated number densities of the relevant species. Number densities for 99 % N_2 and 1 % NH_3 were calculated using the ideal gas law, while those of $N_2(A^3)$ and $N_2(B^3)$ were taken from the chemical analysis in Figure S13. The N_2 and NH_3 number densities represent rough estimates, as production of excited species was not included; however, this does not affect the relative comparison of reaction rates presented.

6. Detailed reaction mechanisms

6.1. Plasma mechanism

Table S15. Overview of the different reactions included in the NH₃/N₂/H₂ plasma reaction mechanism with the references from where the data was adopted. Most electron-impact reactions were treated by energy-dependent cross sections, $f(\sigma)$. Unless otherwise stated, reaction rate coefficients are in the Arrhenius form, for heavy particle collisions: $k = A \times T_{gas}^n \times \exp(-C/T_{gas})$, for electron-impact collisions: $k = A \times T_{e}^n \times \exp(-C/T_{gas})$; both in molecule-cm³-s-K-K units.

No ·	Reaction	Rate coefficient	Ref
Elect	ron impact reactions:		
	Elastic / e	effective / momentum	
1	$e^- + N \rightarrow e^- + N$	f(σ)	28
2	$e^- + H \rightarrow e^- + H$	$f(\sigma)$	29
3	$e^- + N_2 \rightarrow e^- + N_2$	$f(\sigma)$	30,31
4	$e^- + H_2 \rightarrow e^- + H_2$	$f(\sigma)$	30,31
5	$e^- + NH_3 \rightarrow e^- + NH_3$	$f(\sigma)$	32
	Vibra	tional excitation	
6	$e^- + N_2 \rightarrow e^- + N_2 / N_2(v1)$	f(σ)	30,31
7	$e^- + N_2 \to e^- + N_2 / N_2(v2)$	$f(\sigma)$	30,31
8	$e^- + N_2 \to e^- + N_2 / N_2(v3)$	$f(\sigma)$	30,31
9	$e^- + N_2 \to e^- + N_2 / N_2(v4)$	$f(\sigma)$	30,31
10	$e^- + N_2 \to e^- + N_2 / N_2(v5)$	$f(\sigma)$	30,31
11	$e^- + N_2 \to e^- + N_2 / N_2(v6)$	$f(\sigma)$	30,31
12	$e^- + N_2 \to e^- + N_2 / N_2(v7)$	$f(\sigma)$	30,31
13	$e^- + N_2 \to e^- + N_2 / N_2(v8)$	$f(\sigma)$	30,31
14	$e^- + N_2 \to e^- + N_2 / N_2(v9)$	$f(\sigma)$	30,31
15	$e^- + N_2 \rightarrow e^- + N_2 / N_2(v10)$	$f(\sigma)$	30,31
16	$e^- + H_2 \rightarrow e^- + H_2 / H_2(v1j0)$	$f(\sigma)$	30,31
17	$e^- + H_2 \to e^- + H_2 / H_2(v1j2)$	$f(\sigma)$	30,31
18	$e^- + H_2 \to e^- + H_2 / H_2(2v1)$	$f(\sigma)$	30,31
19	$e^- + H_2 \rightarrow e^- + H_2 / H_2(3v1)$	f(\sigma)	30,31
20	$e^- + NH_3 \rightarrow e^- + NH_3 / NH_3(v1)$	f(\sigma)	34 a
21	$e^- + NH_3 \rightarrow e^- + NH_3 / NH_3(v2)$	f(\sigma)	34 a
22	$e^- + NH_3 \rightarrow e^- + NH_3 / NH_3(v31)$	$f(\sigma)$	34 a
23	$e^- + NH_3 \rightarrow e^- + NH_3 / NH_3(v32)$	$f(\sigma)$	34 a
24	$e^- + NH_3 \rightarrow e^- + NH_3 / NH_3(v41)$	$f(\sigma)$	34 a
25	$e^- + NH_3 \rightarrow e^- + NH_3 / NH_3(v42)$	f(o)	34 a
	Electronic ex	citation and dissociation	
26	$e^- + N \rightarrow e^- + N(^2D)$	f(o)	28
27	$e^- + N \rightarrow e^- + N(^2P)$	f(o)	28

28	$e^- + N_2 \longrightarrow e^- + N_2 (A^3) \ / \ N_2 (A^3 \Sigma_u^+)$	$f(\sigma)$	30,31
29	$e^- + N_2 \rightarrow e^- + N_2(B^3) / N_2(B^3\Pi_g)$	$f(\sigma)$	30,31
30	$e^- + N_2 \rightarrow e^- + N_2(B^3) / N_2(B^3\Sigma_u^-)$	$f(\sigma)$	30,31
31	$e^- + N_2 \rightarrow e^- + N_2(B^3) / N_2(W^3 \Delta)$	$f(\sigma)$	30,31
32	$e^- + N_2 \rightarrow e^- + N_2(a^{-1}) / N_2(a^{-1}\Pi_g)$	$f(\sigma)$	30,31
33	$e^- + N_2 \rightarrow e^- + N_2(a^1) / N_2(a^1\Sigma_u^-)$	$f(\sigma)$	30,31
34	$e^- + N_2 \rightarrow e^- + N_2(a^{-1}) / N_2(W^{-1}\Delta)$	$f(\sigma)$	30,31
35	$e^- + N_2 \rightarrow e^- + N_2(C^3) / N2(C^3\Pi_u)$	$f(\sigma)$	30,31
36	$e^- + N_2 \rightarrow e^- + N + N / N_2$ (sum-singlet)	$f(\sigma)$	30,31
37	$e^- + H_2 \rightarrow e^- + H_2 / H_2 (B^{-1}\Sigma_u)$	$f(\sigma)$	33
38	$e^- + H_2 \rightarrow e^- + H_2 / H_2(C \ ^1\Pi_u)$	$f(\sigma)$	33
39	$e^- + H_2 \rightarrow e^- + H_2 / H_2 (E \ ^1\Sigma _g, F \ ^1\Sigma _g)$	$f(\sigma)$	33
40	$e^- + H_2 \rightarrow e^- + H_2 / H_2 (B^{\prime 1}\Sigma_u)$	$f(\sigma)$	33
41	$e^- + H_2 \rightarrow e^- + H_2 / H_2(D^{-1}\Pi_u)$	$f(\sigma)$	33
42	$e^- + H_2 \rightarrow e^- + H_2 / H_2 (B "^1\Sigma_u)$	$f(\sigma)$	33
43	$e^- + H_2 \rightarrow e^- + H_2 / H_2(D^{'1}\Pi_u)$	$f(\sigma)$	33
44	$e^- + H_2 \rightarrow e^- + H_2 / H_2 (G \ ^1\Sigma \ _g^+, \ K \ ^1\Sigma \ _g^+)$	$f(\sigma)$	33
45	$e^- + H_2 \rightarrow e^- + H_2 / H_2 (H {}^1\Sigma_g^+)$	$f(\sigma)$	33
46	$e^- + H_2 \rightarrow e^- + H_2 / H_2 (I^{\ 1}\Pi_{\ g})$	$f(\sigma)$	33
47	$e^- + H_2 \rightarrow e^- + H_2 / H_2 (J^{\ 1}\Delta_{\ g})$	$f(\sigma)$	33
48	$e^- + H_2 \longrightarrow e^- + H + H / H_2 (b\ ^3\Sigma\ _u)$	$f(\sigma)$	33
49	$e^- + H_2 \rightarrow e^- + H + H / H_2(a^3\Sigma_g)$	$f(\sigma)$	33
50	$e^- + H_2 \longrightarrow e^- + H + H / H_2(c^{3}\Pi_u)$	$f(\sigma)$	33
51	$e^- + H_2 \longrightarrow e^- + H + H / H_2(d\ ^3\Pi\ _u)$	$f(\sigma)$	33
52	$e^- + H_2 \longrightarrow e^- + H + H / H_2 (e^{-3}\Sigma_u)$	$f(\sigma)$	33
53	$e^- + H_2 \longrightarrow e^- + H + H / H_2 (h ^3\Sigma _g)$	$f(\sigma)$	33
54	$e^- + H_2 \rightarrow e^- + H + H / H(1s) + H(2p)$	$f(\sigma)$	30,31
55	$e^- + H_2 \rightarrow e^- + H + H / H(1s) + H(2s)$	$f(\sigma)$	30,31
56	$e^- + H_2 \rightarrow e^- + H + H / H(1s) + H(3)$	$f(\sigma)$	30,31
57	$e^- + H_2 \rightarrow e^- + H + H / H(1s) + H(4)$	$f(\sigma)$	30,31
58	$e^- + H_2 \rightarrow e^- + H + H / H(1s) + H(5)$	$f(\sigma)$	30,31
59	$e^- + NH_3 \rightarrow e^- + NH_2 + H / NH_3(e1)$	$f(\sigma)$	34 a
60	$e^- + NH_3 \rightarrow e^- + NH_2 + H / NH_3(e2)$	f(\sigma)	34 a
61	$e^- + NH_3 \rightarrow e^- + NH_2 + H / NH_3(e3)$	f(\sigma)	34 a
62	$e^- + NH_3 \rightarrow e^- + NH_2 + H / NH_3(e4)$	f(o)	34 a
63	$e^- + NH_3 \rightarrow e^- + NH_2 + H / NH_3(e5)$	f(o)	34 a
64	$e^- + NH_3 \rightarrow e^- + NH_2 + H / NH_3(e6)$	$f(\sigma)$	34 a
65	$e^- + NH_3 \rightarrow e^- + NH + H_2 / NH_3(e7)$	$f(\sigma)$	34 a
66	$e^{-} + NH_{3} \rightarrow e^{-} + NH + H_{2} / NH_{3}(e8)$	f(o)	34 a
		Ionization	
67	$e^- + N \rightarrow e^- + e^- + N^+$	f(o)	30,31
68	$e^- + H \longrightarrow e^- + e^- + H^+$	$f(\sigma)$	29
69	$e^- + N_2 \longrightarrow e^- + e^- + N_2^+$	$f(\sigma)$	30,31

$70 e^- + H_2 \longrightarrow e^- + e^- + H_2^+$	$f(\sigma)$	35
71 $e^- + NH \rightarrow e^- + e^- + NH^+$	f(σ)	36
72 $e^- + NH_2 \rightarrow e^- + e^- + NH_2^+$	f(σ)	36
73 $e^- + NH_3 \rightarrow e^- + e^- + NH_3^+$	$f(\sigma)$	36
74 $e^- + H_2 \rightarrow e^- + e^- + H + H^+$	$f(\sigma)$	37
75 $e^- + NH \rightarrow e^- + e^- + H + N^+$	$f(\sigma)$	36
76 $e^- + NH_2 \rightarrow e^- + e^- + H + NH^+$	$f(\sigma)$	36
77 $e^- + NH_3 \rightarrow e^- + e^- + H + NH_2^+$	$f(\sigma)$	36
78 $e^- + NH_3 \rightarrow e^- + e^- + H_2 + NH^+$	$f(\sigma)$	36
79 $e^- + NH_3 \rightarrow e^- + e^- + H + H_2 + N^+$	$f(\sigma)$	36
$80 e^- + NH_3 \rightarrow e^- + e^- + NH_2 + H^+$	$f(\sigma)$	36
$81 e^- + NH_3 \rightarrow e^- + e^- + NH + H_2^+$	$f(\sigma)$	36

Electron-ion recombination:

Lice	non ion recombination.		
82	$e^- + e^- + N^+ \longrightarrow e^- + N$	$7.0 \times 10^{-20} \times (300 / T_{\rm e})^{4.5}$	38
83	$e^- + N^+ + M \longrightarrow N + M$	$6.0 \times 10^{-27} \times (300 / T_{\rm e})^{1.5}$	39
84	$e^- + N_2^+ + M \longrightarrow N_2 + M$	$2.49 \times 10^{-29} \times (T_{\rm e}[{\rm eV}])^{-1.5}$	40
85	$e^- + N_2^+ \longrightarrow N + N$	$0.50 \times 1.8 \times 10^{-7} \times (300 / T_e)^{0.39}$	38
86	$e^- + N_2^+ \longrightarrow N + N(^2D)$	$0.45 \times 1.8 \times 10^{-7} \times (300 / T_e)^{0.39}$	38
87	$e^- + N_2^+ \longrightarrow N + N(^2P)$	$0.05 \times 1.8 \times 10^{-7} \times (300 / T_e)^{0.39}$	38
88	$e^- + e^- + N_2^+ \longrightarrow e^- + N_2$	$1.0 \times 10^{-7} \times (T_{\rm e} / 300)^{-4.5}$	39
89	$e^- + N_3^+ \longrightarrow N_2 + N$	$2.00 \times 10^{-7} \times (300 / T_{\rm e})^{0.5}$	38
90	$e^- + N_3^+ \rightarrow N_2(A^3) + N$	$6.91 \times 10^{-8} \times (300 / T_{\rm e} [{ m eV}])^{-0.5}$	40
91	$e^- + N_3^+ \rightarrow N_2(B^3) + N$	$6.91 \times 10^{-8} \times (300 / T_{\rm e}[{\rm eV}])^{-0.5}$	40
92	$e^- + N_4^+ \longrightarrow N_2 + N_2$	$2.30 \times 10^{-6} \times (300 / T_{\rm e})^{0.53}$	38
93	$e^- + N_4^+ \longrightarrow N_2 + N + N$	$3.13 \times 10^{-7} \times (T_{\rm e}[{\rm eV}])^{-0.41}$	40
94	$e^- + H_2^+ \longrightarrow H + H$	\mathbf{k}_{al}	41 b
95	$e^- + H_3^+ \longrightarrow H + H + H$	k_{a2}	41 b
96	$e^- + H_3^+ \longrightarrow H_2 + H$	k_{a2}	41 b
97	$e^- + NH^+ \longrightarrow N + H$	$4.30 \times 10^{-8} \times (0.026 / T_{\rm e} [{\rm eV}])^{0.5}$	41
98	$e^- + NH_2^+ \longrightarrow NH + H$	$1.02 \times 10^{-7} \times (0.026 / T_{\rm e} [{\rm eV}])^{0.4}$	41
99	$e^- + NH_2^+ \longrightarrow N + H + H$	$1.98 \times 10^{-7} \times (0.026 / T_{\rm e} [{\rm eV}])^{0.4}$	41
100	$e^- + NH_3^+ \longrightarrow NH + H + H$	$1.55 \times 10^{-7} \times (0.026 / T_{\rm e} [{\rm eV}])^{0.5}$	41
101	$e^- + NH_3^+ \longrightarrow NH_2 + H$	$1.55 \times 10^{-7} \times (0.026 / T_{\rm e} [{\rm eV}])^{0.5}$	41
102	$e^- + NH_4^+ \longrightarrow NH_3 + H$	$8.01 \times 10^{-7} \times (0.026 / T_{e} [eV])^{0.605}$	41
103	$e^- + NH_4^+ \longrightarrow NH_2 + H + H$	$1.23 \times 10^{-7} \times (0.026 / T_e[eV])^{0.605}$	41

Neutral-neutral reactions:

Reactio	ons with excited species	
$104 N(^2D) + M \rightarrow N + M$	2.40×10^{-14}	42
105 $N(^{2}P) + N \rightarrow N(^{2}D) + N$	1.80×10^{-12}	38
106 $N(^{2}P) + N_{2} \rightarrow N + N_{2}$	2.00×10^{-18}	38
107 $N_2(a^1) + N \rightarrow N_2 + N$	2.00×10^{-11}	42

108	$N_2(a^1) + N_2 \rightarrow N_2 + N_2$	3.70×10^{-16}	42
109	$N_2(a^1) + N_2 \rightarrow N_2(B^3) + N_2$	1.90×10^{-13}	38
110	$N_2(A^3) + N \rightarrow N_2 + N$	2.00×10^{-12}	38
111	$N_2(A^3) + N \rightarrow N_2 + N(^2P)$	$4.00 \times 10^{-11} \times (300 / T_{\rm gas})^{0.667}$	38
112	$N_2(A^3) + N_2 \rightarrow N_2 + N_2$	3.00×10^{-16}	38
113	$N_2(A^3) + N_2(A^3) \rightarrow N_2 + N_2(A^3)$	2.00×10^{-12}	42
114	$N_2(A^3) + N_2(A^3) \rightarrow N_2 + N_2(B^3)$	4.20×10^{-11}	Based on 43,44
115	$N_2(A^3) + N_2(A^3) \rightarrow N_2 + N_2(C^3)$	9.00×10^{-11}	Based on 43,44
116	$N_2(A^3) + N_2(A^3) \rightarrow N_2 + N + N$	1.25×10^{-10}	Based on 43,44
117	$N_2(B^3) + N_2 \rightarrow N_2 + N_2$	2.00×10^{-12}	38
118	$N_2(B^3) + N_2 \rightarrow N_2(A^3) + N_2$	3.00×10^{-11}	38
119	$N_2(C^3) + N_2 \rightarrow N_2(a^1) + N_2$	1.00×10^{-11}	38
120	$N_2(a^{-1}) + N_2(a^{-1}) \rightarrow e^- + N_2^+ + N_2$	5.00×10^{-13}	42
121	$N_2(a^{-1}) + N_2(a^{-1}) \rightarrow e^- + N_4^+$	1.00×10^{-11}	38
122	$N_2(a^{-1}) + N_2(a^{-1}) \rightarrow e^- + N_4^+$	4.00×10^{-12}	38
123	$N_2(A^3) + N_2(a^1) \rightarrow e^- + N_2 + N_2^+$	1.00×10^{-12}	42
124	$N_2(A^3) + H \rightarrow N_2 + H$	5.00×10^{-11}	44
125	$N_2(A^3) + H_2 \rightarrow N_2 + H + H$	$2.00 \times 10^{-10} \times \exp(-3500 / T_{\rm gas})$	44
126	$N_2(B^3) + H_2 \rightarrow N_2(A^3) + H_2$	2.50×10^{-11}	44
127	$N_2(a^1) + H \rightarrow N_2 + H$	1.50×10^{-11}	44
128	$N_2(a^1) + H_2 \rightarrow N_2 + H + H$	2.60×10^{-11}	44
129	$N_2(A^3) + NH_3 \rightarrow N_2 + NH_2 + H$	1.20×10^{-10}	45
130	$N_2(a^1) + NH_3 \rightarrow N_2 + NH_2 + H$	1.20×10^{-10}	Analogy as 8
131	$N(^2D) + H_2 \rightarrow H + NH$	2.30×10^{-12}	44
132	$N(^2D) + NH_3 \rightarrow NH + NH_2$	1.10×10^{-10}	44
133	$N(^2P) + H_2 \rightarrow H + NH$	2.50×10^{-14}	44

Ion-neutral reactions:

		Two-body collisions	
13	$34 N^+ + H_2 \rightarrow NH^+ + H$	5.00×10^{-10}	46
13	$35 N^+ + NH_3 \rightarrow NH_2^+ + NH$	$0.20 \times 2.35 \times 10^{-9}$	46
13	$36 N^+ + NH_3 \rightarrow NH_2^+ + N$	$0.71 \times 2.35 \times 10^{-9}$	46
13	$37 N^+ + NH_3 \rightarrow NNH^+ + H_2$	$0.09 \times 2.35 \times 10^{-9}$	46
13	$38 N_2^+ + N \to N^+ + N_2$	$7.20 \times 10^{-13} \times (T_{\text{ion}} / 300)$	38 c
13	39 $N_2^+ + H_2 \rightarrow NNH^+ + H$	2.00×10^{-9}	41
14	$40 N_2^+ + N_2(A^3) \to N_3^+ + N$	3.00×10^{-10}	47
14	$11 N_2^+ + NH_3 \rightarrow NH_3^+ + N_2$	1.95×10^{-9}	41
14	$42 N_3^+ + N \to N_2^+ + N_2$	6.60×10^{-11}	38
14	43 $N_4^+ + N \rightarrow N^+ + N_2 + N_2$	1.00×10^{-11}	38
14	44 $H^+ + NH_3 \rightarrow NH_3^+ + H$	5.20×10^{-9}	46
14	45 $H_2^+ + H \rightarrow H^+ + H_2$	$6.40 imes 10^{-10}$	41
14	$46 \text{H}_2^+ + \text{H}_2 \longrightarrow \text{H}_3^+ + \text{H}$	2.00×10^{-9}	41
14	47 $H_2^+ + N_2 \rightarrow NNH^+ + H$	2.00×10^{-9}	46

148	$H_2^+ + NH_3 \rightarrow NH_3^+ + H_2$	5.70×10^{-9}	46
149	$NH^+ + H_2 \rightarrow H_3^+ + N$	$0.15 \times 1.23 \times 10^{-9}$	46
150	$NH^+ + H_2 \rightarrow NH_2^+ + H$	$0.85 \times 1.23 \times 10^{-9}$	46
151	$NH^+ + NH_3 \rightarrow NH_3^+ + NH$	$0.75 \times 2.40 \times 10^{-9}$	46
152	$NH^+ + NH_3 \rightarrow NH_4^+ + N$	$0.25 \times 2.40 \times 10^{-9}$	46
153	$NH^+ + N_2 \rightarrow NNH^+ + N$	6.50×10^{-9}	46
154	$NH_2^+ + H_2 \rightarrow NH_3^+ + H$	1.95×10^{-9}	46
155	$NH_2^+ + NH_3 \rightarrow NH_3^+ + NH_2$	$0.5 \times 2.30 \times 10^{-9}$	46
156	$NH_2^+ + NH_3 \rightarrow NH_4^+ + NH$	$0.5 \times 2.30 \times 10^{-9}$	46
157	$NH_3^+ + NH_3 \rightarrow NH_4^+ + NH_2$	2.10×10^{-9}	46
158	$NNH^+ + NH_3 \rightarrow NH_4^+ + N_2$	2.30×10^{-9}	46
159	$N+N \longrightarrow e^- + N_2{}^+$	$2.70 \times 10^{-11} \times \exp(-67400 / T_{\rm g})$	38
		Three-body collisions	
160	$N + N + N \rightarrow N_2(A^3) + N$	1.0×10^{-32}	38
161	$N + N + N \rightarrow N_2(B^3) + N$	1.4×10^{-32}	38
162	$N + N + N_2 \rightarrow N_2(A^3) + N_2$	1.7×10^{-33}	38
163	$N + N + N_2 \rightarrow N_2(B^3) + N_2$	2.4×10^{-33}	38
164	$N+H+M \rightarrow NH+M$	$(1/380) \times 1.0 \times 10^{-33}$	38
165	$N + H_2 + M \longrightarrow NH_2 + M$	$(1/380) \times 1.0 \times 10^{-34}$	38
166	$N + N + H \rightarrow N_2(A^3) + H$	$(1/380) \times 1.0 \times 10^{-32}$	38
167	$N + N + H \rightarrow N_2(B^3) + H$	$(1/380) \times 1.4 \times 10^{-32}$	38
168	$N + N + H_2 \rightarrow N_2(A^3) + H_2$	$(1/380) \times 1.7 \times 10^{-33}$	38
169	$N + N + H_2 \rightarrow N_2(B^3) + H_2$	$(1/380) \times 2.4 \times 10^{-33}$	38
170	$N_2^+ + N + N_2 \longrightarrow N_3^+ + N_2$	$9.00 \times 10^{-30} \times \exp(400 / T_{\text{ion}})$	38 c
171	$N^+ + N_2 + N_2 \longrightarrow N_3^+ + N_2$	$1.70 \times 10^{-29} \times (300 / T_{\text{ion}})^{2.1}$	38 c
172	$N_2^+ + N_2 + N_2 \longrightarrow N_4^+ + N_2$	$5.20 \times 10^{-29} \times (300 / T_{\text{ion}})^{2.2}$	38 c
173	$N^+ + N + N_2 \rightarrow N_2^+ + N_2$	5.20×10^{-29}	38
		Radiative decay	
174	$N_2(A^3) \rightarrow N_2$	0.5	38
175	$N_2(B^3) \rightarrow N_2(A^3)$	1.34×10^{5}	38
176	$N_2(a^1) \rightarrow N_2$	1.00×10^2	38
177	$N_2(C^3) \rightarrow N_2(B^3)$	2.45×10^{7}	38

^a Reaction rate coefficients are newly updated compared to old mechanism ⁸.

The reaction rate coefficients k_{a1} , k_{a2} are fitted as a function of electron temperature: $k_{a1} = 7.51 \times 10^{-9} - 1.12 \times 10^{-9} T_e [\text{eV}]^1 + 1.03 \times 10^{-10} T_e [\text{eV}]^2 - 4.15 \times 10^{-12} T_e [\text{eV}]^3 + 5.86 \times 10^{-14} T_e [\text{eV}]^4$ $k_{\rm a2} = 0.5 \times (8.39 \times 10^{-9} + 3.02 \times 10^{-9} T_e [\rm eV]^1 - 3.80 \times 10^{-10} T_e [\rm eV]^2 + 1.31 \times 10^{-11} T_e [\rm eV]^3 + 2.42 \times 10^{-13} T_e [\rm eV]^4 - 2.30 \times 10^{-14} T_e [\rm eV]^5 + 3.55 \times 10^{-16} T_e [\rm eV]^6)$ Can effective ion temperature $T_{\rm ion}$ is used 38.

6.2. Thermal mechanism modified from PCMech-1 in Bang et al.⁸

Table S16. Overview of the different reactions included in the NH₃/N₂/H₂ thermal reaction mechanism modified from PCMech-1 in Bang et al.⁸ Newly-added reactions are indicated with separate references. The reaction rate coefficients are in the Arrhenius form: $k = A \times T_{gas}^n \times \exp(-E_a / R \times T_g)$, in mol-cm³-s-cal-K units.

Conventional (thermal) reactions:

Con	ventional (thermal) reactions.		
1	$H_2 + M \rightarrow H + H + M$	$4.60 \times 10^{19} \times {T_{\rm gas}}^{-1.4} \times \exp(-1.04380 \times 10^5 / R \times T_{\rm gas})$ H ₂ enhanced by 2.50	
2	$H + H + M \rightarrow H_2 + M$	Reverse reaction rate	
3	$N + N + M \rightarrow N_2 + M$	$5.01 \times 10^{14} \times \exp(1.000 \times 10^3 / R \times T_{\rm gas})$	48
4	$N_2 + M \rightarrow N + N + M$	Reverse reaction rate	
5	$NH + H \rightarrow N + H_2$	$1.65 \times 10^{11} \times T_{\rm gas}^{0.71} \times \exp(9.31 \times 10^2 / R \times T_{\rm gas})$	
6	$N + H_2 \rightarrow NH + H$	Reverse reaction rate	
7	$NH + NH \rightarrow N_2 + H_2$	$6.26 \times 10^{12} \times T_{\rm gas}^{-0.036} \times \exp(-160.9 / R \times T_{\rm gas})$	
8	$NH + NH \rightarrow N_2 + H + H$	$5.634 \times 10^{13} \times T_{\rm gas}^{-0.036} \times \exp(-160.9 / R \times T_{\rm gas})$	
9	$NH + N \rightarrow N_2 + H$	3.00×10^{13}	
10	$N_2 + H \rightarrow NH + N$	Reverse reaction rate	
11	$NH_2 + M \rightarrow NH + H + M$	$1.20 \times 10^{15} \times \exp(7.6002 \times 10^4 / R \times T_{\rm gas})$	
12	$NH + H + M \rightarrow NH_2 + M$	Reverse reaction rate	
13	$NH_2 + H \rightarrow NH + H_2$	$1.09 \times 10^5 \times T_{\rm gas}^{2.59} \times \exp(1.81232 \times 10^3 / R \times T_{\rm gas})$	
14	$NH + H_2 \rightarrow NH_2 + H$	Reverse reaction rate	
15	$NH_2 + N \rightarrow N_2 + H + H$	6.90×10^{13}	
16	$N_2 + H + H \rightarrow NH_2 + N$	Reverse reaction rate	
17	$NH + NH \rightarrow NH_2 + N$	$0.570 imes T_{ m gas}^{3.88} imes \exp(342 / R imes T_{ m gas})$	
18	$NH_2 + N \rightarrow NH + NH$	Reverse reaction rate	
19	$NH_2 + NH_2 \rightarrow NH_3 + NH$	$5.636 \times T_{\rm gas}^{3.53} \times \exp(552.6 / R \times T_{\rm gas})$	
20	$NH_3 + NH \rightarrow NH_2 + NH_2$	Reverse reaction rate	
21	$NH_2 + NH \rightarrow NH_3 + N$	$9.574 \times 10^3 \times T_{\rm gas}^{2.46} \times \exp(107.3 / R \times T_{\rm gas})$	
22	$NH_3 + N \rightarrow NH_2 + NH$	Reverse reaction rate	
23	$N_2H_2 + H \rightarrow NNH + H_2$	$4.820 \times 10^8 \times T_{\rm gas}^{1.76} \times \exp(739.2 / R \times T_{\rm gas})$	
24	$NNH + H_2 \rightarrow N_2H_2 + H$	Reverse reaction rate	
25	$N_2H_2 + NH \rightarrow NNH + NH_2$	$2.40 \times 10^6 \times T_{\rm gas}^{2.00} \times \exp(-1.192 \times 10^3 / R \times T_{\rm gas})$	
26	$NNH + NH_2 \rightarrow N_2H_2 + NH$	Reverse reaction rate	
27	$N_2H_2 + NH_2 \rightarrow NNH + NH_3$	$2.71 \times 10^5 \times T_{\rm gas}^{2.226} \times \exp(-1.03 \times 10^3 / R \times T_{\rm gas})$	
28	$NNH + NH_3 \rightarrow N_2H_2 + NH_2$	Reverse reaction rate	
29	$NH_2 + NH \rightarrow N_2H_2 + H$	$1.30 \times 10^{14} \times T_{\rm gas}^{-0.272} \times \exp(-77 / R \times T_{\rm gas})$	
30	$N_2H_2 + H \rightarrow NH_2 + NH$	Reverse reaction rate	
31	$NH_2 + NH_2 \longrightarrow N_2H_2 + H_2$	$1.70 \times 10^8 \times T_{\rm gas}^{1.620} \times \exp(1.1783 \times 10^4 / R \times T_{\rm gas})$	
32	$N_2H_2 + H_2 \rightarrow NH_2 + NH_2$	Reverse reaction rate	
33	$NH_2 + NH_2 (+M) \rightarrow N_2H_4 (+M)$	$5.60 \times 10^{14} \times T_{\text{gas}}^{-0.414} \times \exp(66 / R \times T_{\text{gas}})$	
		LOW / $1.60 \times 10^{34} \times T_{\text{gas}}^{-5.49} \times \exp(1.987 \times 10^3 / R \times T_{\text{gas}})$	
		TROE / $0.31\ 1.0 \times 10^{-30}\ 1.0 \times 10^{30}\ 1.0 \times 10^{30}$ N ₂ enhanced by 1.00	
		NH ₃ enhanced by 4.87	
		- •	

34 N_2H_4 (+M) $\rightarrow NH_2 + NH_2$ (+M)

- 35 $N_2H_4 \rightarrow N_2H_2 + H_2$
- 36 $N_2H_2 + H_2 \rightarrow N_2H_4$ Reaction excluded
- $37 N_2H_4 \rightarrow N_2H_3 + H$
- 38 $N_2H_3 + H \rightarrow N_2H_4$ Reaction excluded
- 39 $N_2H_4 + H \rightarrow N_2H_3 + H_2$
- $40 N_2H_3 + H_2 \rightarrow N_2H_4 + H$
- 41 $N_2H_4 + NH_2 \rightarrow N_2H_3 + NH_3$
- 42 $N_2H_3 + NH_3 \rightarrow N_2H_4 + NH_2$
- 43 $N_2H_4 + N_2H_2 \rightarrow N_2H_3 + N_2H_3$
- 44 $N_2H_3 + N_2H_3 \rightarrow N_2H_4 + N_2H_2$
- 45 $N_2H_4 + NH \rightarrow N_2H_3 + NH_2$
- 46 $N_2H_3 + NH_2 \rightarrow N_2H_4 + NH$
- 47 N_2H_3 (+M) $\rightarrow N_2H_2 + H$ (+M)
- 48 $N_2H_2 + H (+M) \rightarrow N_2H_3 (+M)$
- 49 $N_2H_3 + H \rightarrow N_2H_2 + H_2$
- 50 $N_2H_2 + H_2 \rightarrow N_2H_3 + H$
- 51 $N_2H_3 + H \rightarrow H_2NN + H_2$
- $52 \quad H_2NN + H_2 \rightarrow N_2H_3 + H$
- 53 $N_2H_3 + H \rightarrow NH_3 + NH$
- 54 $NH_3 + NH \rightarrow N_2H_3 + H$
- 55 $N_2H_3 + NH_2 \rightarrow N_2H_2 + NH_3$
- $56 \quad N_2H_2 + NH_3 \rightarrow N_2H_3 + NH_2$
- 57 $N_2H_3 + NH_2 \rightarrow H_2NN + NH_3$
- 58 $H_2NN + NH_3 \rightarrow N_2H_3 + NH_2$
- 59 $N_2H_3 + NH \rightarrow N_2H_2 + NH_2$
- $60 \quad N_2H_2 + NH_2 \rightarrow N_2H_3 + NH$
- 61 $N_2H_3 + N_2H_2 \rightarrow N_2H_4 + NNH$
- 62 $N_2H_4 + NNH \rightarrow N_2H_3 + N_2H_2$
- 63 $N_2H_3 + N_2H_3 \rightarrow NH_3 + NH_3 + N_2$
- 64 $NH_3 + NH_3 + N_2 \rightarrow N_2H_3 + N_2H_3$
- 65 $N_2H_2 + N_2H_2 \rightarrow N_2H_3 + NNH$
- 66 $N_2H_3 + NNH \rightarrow N_2H_2 + N_2H_2$
- $67 \quad NH_2 + NH_2 \rightarrow H_2NN + H_2$
- $68 \quad H_2NN + H_2 \rightarrow NH_2 + NH_2$
- 69 $H_2NN \rightarrow NNH + H$
- 70 NNH + H \rightarrow H₂NN
- 71 $H_2NN + H \rightarrow NNH + H_2$

Reverse reaction rate

$$5.19 \times 10^{38} \times T_{\rm gas}^{-7.84} \times \exp(6.71 \times 10^4 / R \times T_{\rm gas})$$

Reverse reaction rate

$$2.74 \times 10^{39} \times T_{\text{gas}}^{-7.69} \times \exp(8.37 \times 10^4 / R \times T_{\text{gas}})$$

Reverse reaction rate

$$2.76 \times 10^5 \times T_{\rm gas}^{2.56} \times \exp(1.22 \times 10^3 / R \times T_{\rm gas})$$

Reverse reaction rate

$$3.96 \times 10^{12} \times \exp(1.50 \times 10^3 / R \times T_{\rm gas})$$

Reverse reaction rate

$$2.50 \times 10^{10} \times T_{\rm gas}^{0.5} \times \exp(2.98 \times 10^4 / R \times T_{\rm gas})$$

Reverse reaction rate

$$1.00 \times 10^{12} \times \exp(1.99 \times 10^3 / R \times T_{\rm gas})$$

Reverse reaction rate

$$1.28 \times 10^{11} \times T_{\rm gas}^{0.819} \times \exp(4.81 \times 10^4 / R \times T_{\rm gas})$$

LOW /
$$3.84 \times 10^{40} \times T_{\rm gas}^{-6.88} \times \exp(5.45 \times 10^4 / R \times T_{\rm gas})$$

TROE / $0.8428.0 \times 10^4287.298 \times 10^3$

N₂ enhanced by 2.00

Reverse reaction rate

$$7.476 \times 10^3 \times T_{\text{gas}}^{2.796} \times \exp(4.68 \times 10^3 / R \times T_{\text{gas}})$$

Reverse reaction rate

$$6.243 \times 10^6 \times T_{\rm gas}^{1.89} \times \exp(2.47 \times 10^2 / R \times T_{\rm gas})$$

Reverse reaction rate

$$1.00\times10^{11}$$

Reverse reaction rate

$$0.608 \times T_{\rm gas}^{3.574} \times \exp(1.19 \times 10^3 / R \times T_{\rm gas})$$

Reverse reaction rate

$$11.1 \times T_{\rm gas}^{3.08} \times \exp(2.11 \times 10^2 / R \times T_{\rm gas})$$

Reverse reaction rate

$$2.00 \times 10^{13}$$

Reverse reaction rate

$$1.00 \times 10^{13} \times \exp(9.94 \times 10^3 / R \times T_{\text{gas}})$$

Reverse reaction rate

$$3.00\times10^{12}$$

Reverse reaction rate

$$1.00 \times 10^{13} \times \exp(9.935 \times 10^3 / R \times T_{\text{gas}})$$

Reverse reaction rate

$$7.20 \times 10^4 \times T_{\rm gas}^{1.88} \times \exp(8.802 \times 10^3 / R \times T_{\rm gas})$$

Reverse reaction rate

$$3.40 \times 10^{26} \times T_{\rm gas}^{-4.83} \times \exp(4.622 \times 10^4 / R \times T_{\rm gas})$$

Reverse reaction rate

$$4.80 \times 10^8 \times T_{\rm gas}^{1.50} \times \exp(-8.94 \times 10^2 / R \times T_{\rm gas})$$

72	$NNH + H_2 \rightarrow H_2NN + H$	Reverse reaction rate	
73	$H_2NN + H \rightarrow N_2H_2 + H$	7.00×10^{13}	
74	$N_2H_2 + H \rightarrow H_2NN + H$	Reverse reaction rate	
75	$H_2NN + NH_2 \rightarrow NNH + NH_3$	$1.80 \times 10^6 \times T_{\rm gas}^{1.94} \times \exp(-1.152 \times 10^3 / R \times T_{\rm gas})$	
76	$NNH + NH_3 \rightarrow H_2NN + NH_2$	Reverse reaction rate	
77	$NH_3 + M \rightarrow NH_2 + H + M$	$6.25 \times 10^{15} \times T_{\rm gas}^{0.69} \times \exp(-1.0041 \times 10^5 / R \times T_{\rm gas})$	a
		H ₂ enhanced by 2.50	
		NH ₃ enhanced by 4.76	
78	$NH_2 + H + M \rightarrow NH_3 + M$	Reverse reaction rate	
79	$NH_3 + H \rightarrow NH_2 + H_2$	$2.89 \times 10^6 \times T_{\rm gas}^{2.23} \times \exp(1.04 \times 10^4 / R \times T_{\rm gas})$	
80	$NH_2 + H_2 \rightarrow NH_3 + H$	Reverse reaction rate	
81	$NH_3 + NH_2 \rightarrow N_2H_3 + H_2$	$1.00 \times 10^{11} \times T_{\rm gas}^{0.50} \times \exp(2.16 \times 10^4 / R \times T_{\rm gas})$	
82	$N_2H_3 + H_2 \rightarrow NH_3 + NH_2$	Reverse reaction rate	
83	$NNH \rightarrow N_2 + H$	3.30×10^{8}	
84	$N_2 + H \rightarrow NNH$	Reverse reaction rate	
85	$NNH + H \rightarrow N_2 + H_2$	1.00×10^{14}	
86	$N_2 + H_2 \rightarrow NNH + H$	Reverse reaction rate	
87	$NNH + NH \rightarrow N_2 + NH_2$	5.00×10^{13}	
88	$N_2 + NH_2 \rightarrow NNH + NH$	Reverse reaction rate	
89	$NNH + NH_2 \rightarrow N_2 + NH_3$	5.00×10^{13}	
90	$N_2 + NH_3 \rightarrow NNH + NH_2$	Reverse reaction rate	
91	$NNH + NNH \rightarrow N_2H_2 + N_2$	$1.00 \times 10^{13} \times \exp(9.935 \times 10^3 / R \times T_{\rm gas})$	
92	$N_2H_2 + N_2 \rightarrow NNH + NNH$	Reverse reaction rate	

^a The reaction rate coefficient is acquired by the curve-fitting as Figure S25.

In the revised mechanism, the following reaction rate coefficients were updated:

1. Electron-impact reactions of NH₃.

The earlier mechanism included only three electron-impact reactions for NH₃, owing to the lack of data at the time. In the meantime, a recent study by Snoeckx et al.³⁴ has provided a comprehensive cross section dataset for electron-impact reactions with NH₃, which was adopted here.

2. Recombination reaction between NH2 and H.

Based on our previous work⁸, the recombination reaction, $NH_2+H(+M) \rightarrow NH_3(+M)$ consistently appears as one of the most sensitive reactions across different reaction mechanisms tested. Moreover, its rate coefficient has a high uncertainty, particularly under low-temperature conditions

 $(T_{\rm g}$ < 1000 K). However, since no experimental measurements are available, we estimated this rate using three parameters fitting based on two different coefficients reported by Davidson et al.⁴⁹ and Altinay & McDonald⁵⁰ in the literature (see Figure S30). The replacement of this reaction rate significantly improved the predictive performance of our model (Figure S8 and S9).

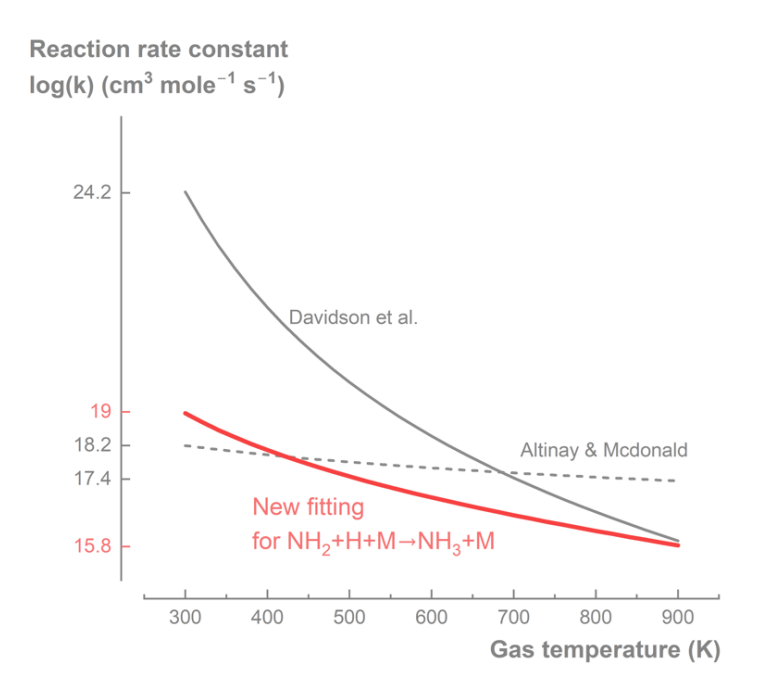


Figure S30. The reaction rate constant was obtained by curve-fitting, using rate constants reported by Davidson et al.⁴⁹ and Altinay & McDonald⁵⁰.

The sensitivity analysis with the updated reaction mechanism (Figure S31) reconfirms the critical importance of the $NH_2 + H$ recombination reaction, supporting the motivation for this update. In addition, electron-impact dissociation of N_2 and the reactions of NH_2 with N also emerge as key reactions. In particular, the latter reactions between NH_2 and N should be highlighted, as their rate coefficients are outdated and were measured only at a single temperature point (300 K). By contrast, the rate coefficients for electron-impact processes of N_2 (i.e., cross-section data) have been extensively studied and are therefore considered more reliable.

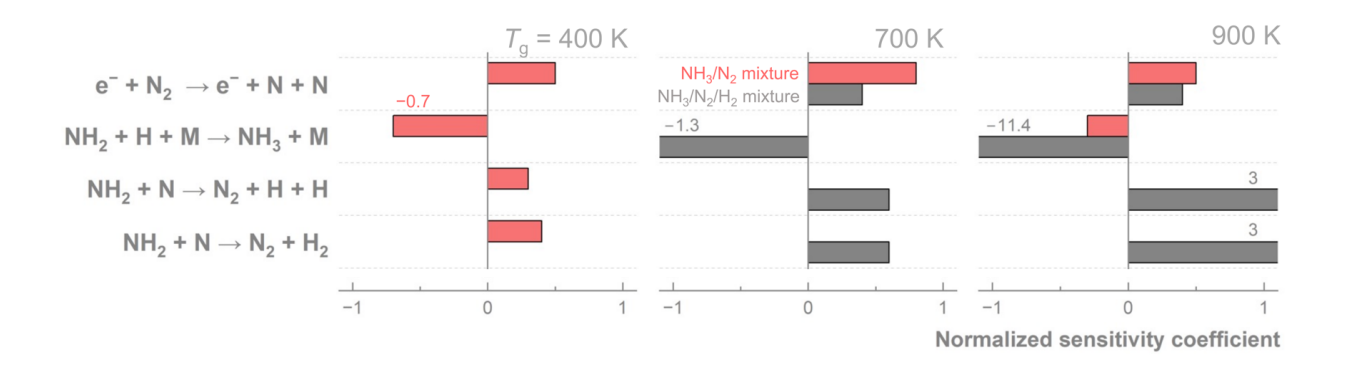


Figure S31. Sensitivity analysis with the updated reaction mechanism at three representative gas temperatures: 400 K, 700 K, and 900 K. Red bars indicate the NH₃/N₂ mixture, while gray bars correspond to NH₃/N₂/H₂ (N₂:H₂ = 1:3). Sensitivity analysis for NH₃/H₂ is not shown, as the model predicts nearly zero conversion under all simulated conditions. In this case, the normalized sensitivity coefficients would be mathematically exaggerated and lack physical significance.

7. References

 Pipa, A. & Brandenburg, R. The Equivalent Circuit Approach for the Electrical Diagnostics of Dielectric Barrier Discharges: The Classical Theory and Recent Developments. *Atoms* 7, 14 (2019).

- 2. Manley, T. C. The Electric Characteristics of the Ozonator Discharge. *Transactions of The Electrochemical Society* **84**, 83 (1943).
- Peeters, F. & Butterworth, T. Electrical Diagnostics of Dielectric Barrier Discharges. in *Atmospheric Pressure Plasma from Diagnostics to Applications* 1–27 (IntechOpen, 2019).
 doi:10.5772/intechopen.80433.
- 4. Raizer, Y. P. Gas Discharge Physics. (Springer Berlin Heidelberg, Berlin, Heidelberg, 1997).
- 5. Zhang, X. & Cha, M. S. Electron-induced dry reforming of methane in a temperature-controlled dielectric barrier discharge reactor. *Journal of Physics D: Applied Physics* **46**, 415205 (2013).
- 6. Xie, X., Cheng, Y., Wu, K. & Xiao, B. Study on α-β quartz phase transition and its effect on dielectric properties. *Journal of Applied Physics* **111**, 104116 (2012).
- 7. Peeters, F. J. J. & Van De Sanden, M. C. M. The influence of partial surface discharging on the electrical characterization of DBDs. *Plasma Sources Sci. Technol.* **24**, 015016 (2014).
- 8. Bang, S., Snoeckx, R. & Cha, M. S. Kinetic Study for Plasma Assisted Cracking of NH3: Approaches and Challenges. *J. Phys. Chem. A* (2023) doi:10.1021/acs.jpca.2c06919.
- 9. Vanraes, P., Nikiforov, A., Bogaerts, A. & Leys, C. Study of an AC dielectric barrier single micro-discharge filament over a water film. *Sci Rep* **8**, 10919 (2018).
- 10. Yoshida, K., Komuro, A. & Ando, A. Effects of relative permittivity on primary and secondary streamers in atmospheric pressure dielectric barrier discharge. *J. Phys. D: Appl. Phys.* **54**, 315203 (2021).

11. Jovanović, A. P., Hoder, T., Höft, H., Loffhagen, D. & Becker, M. M. Formation mechanisms of striations in a filamentary dielectric barrier discharge in atmospheric-pressure argon. *Plasma Sources Sci. Technol.* **32**, 055011 (2023).

- 12. Chen, S. *et al.* Measurement of inhomogeneous electric field based on electric field-induced second-harmonic generation. *Measurement* **231**, 114576 (2024).
- 13. Chen, T. Y. *et al.* Quantitative time-resolved diagnostics of electric field dynamics during individual plasma breakdown events using burst laser pulse electric field induced second harmonic generation. *Appl. Phys. Lett.* **125**, 054102 (2024).
- 14. Guo, Y., Limburg, A., Laarman, J., Teunissen, J. & Nijdam, S. Measurement of the electric field distribution in streamer discharges. *Phys. Rev. Res.* **7**, 013051 (2025).
- Mohanan, A., Snoeckx, R. & Cha, M. S. Temperature-Dependent Kinetics of Plasma-Based CO₂
 Conversion: Interplay of Electron-Driven and Thermal-Driven Chemistry. *ChemSusChem* e202401526 (2024) doi:10.1002/cssc.202401526.
- Bang, S., Snoeckx, R. & Cha, M. S. Temperature-Dependent Kinetics of Ozone Production in Oxygen Discharges. *Plasma Chem Plasma Process* (2023) doi:10.1007/s11090-023-10370-7.
- 17. Snoeckx, R., Jun, D., Lee, B. J. & Cha, M. S. Kinetic study of plasma assisted oxidation of H2 for an undiluted lean mixture. *Combustion and Flame* **242**, 112205 (2022).
- 18. Snoeckx, R. & Cha, M. S. Kinetic study of plasma assisted oxidation of H2 for an undiluted rich mixture. *Combustion and Flame* **250**, 112638 (2023).
- 19. Ozkan, A. *et al.* The influence of power and frequency on the filamentary behavior of a flowing DBD—application to the splitting of CO₂. *Plasma Sources Sci. Technol.* **25**, 025013 (2016).

20. Motret, O., Pellerin, S., Nikravech, M., Massereau, V. & Pouvesle, J. M. Spectroscopic Characterization of CH4 + CO2 Plasmas Excited by a Dielectric Barrier Discharge at Atmospheric Pressure. *Plasma Chemistry and Plasma Processing* 17, 393–407 (1997).

- 21. Motret, O., Hibert, C., Pellerin, S. & Pouvesle, J. M. Rotational temperature measurements in atmospheric pulsed dielectric barrier discharge gas temperature and molecular fraction effects. *Journal of Physics D: Applied Physics* 33, 1493–1498 (2000).
- 22. Aerts, R., Somers, W. & Bogaerts, A. Carbon Dioxide Splitting in a Dielectric Barrier Discharge Plasma: A Combined Experimental and Computational Study. *ChemSusChem* **8**, 702–716 (2015).
- 23. Snoeckx, R., Aerts, R., Tu, X. & Bogaerts, A. Plasma-Based Dry Reforming: A Computational Study Ranging from the Nanoseconds to Seconds Time Scale. *The Journal of Physical Chemistry C* 117, 4957–4970 (2013).
- 24. Jidenko, N., Bourgeois, E. & Borra, J.-P. Temperature profiles in filamentary dielectric barrier discharges at atmospheric pressure. *Journal of Physics D: Applied Physics* **43**, 295203 (2010).
- 25. Lepikhin, N. D., Popov, N. A. & Starikovskaia, S. M. Fast gas heating and radial distribution of active species in nanosecond capillary discharge in pure nitrogen and N2:O2 mixtures. *Plasma Sources Sci. Technol.* **27**, 055005 (2018).
- 26. Hagelaar, G. J. M. & Pitchford, L. C. Solving the Boltzmann equation to obtain electron transport coefficients and rate coefficients for fluid models. *Plasma Sources Science and Technology* 14, 722–733 (2005).
- 27. Šimek, M. Optical diagnostics of streamer discharges in atmospheric gases. *J. Phys. D: Appl. Phys.* **47**, 463001 (2014).
- 28. Wang, Y., Zatsarinny, O. & Bartschat, K. B-spline R-matrix-with-pseudostates calculations for electron-impact excitation and ionization of nitrogen. *Physical Review A* **89**, 062714 (2014).

29. Morgan, L. W. Morgan (Kinema Research Software) database. www.lxcat.net/Morgan.

- 30. Alves, L. L. The IST-Lisbon database on LXCat. J. Phys. Conf. Series 565, 1 (2014).
- 31. Alves, L. L. IST-Lisbon database. www.lxcat.net/IST-Lisbon.
- 32. Hayashi, M. Hayashi database. www.lxcat.net/Hayashi.
- 33. Zammit, M. C., Savage, J. S., Fursa, D. V. & Bray, I. Electron-impact excitation of molecular hydrogen. *Phys. Rev. A* **95**, 022708 (2017).
- 34. Snoeckx, R., Tennyson, J. & Cha, M. S. Theoretical cross sections for electron collisions relevant for ammonia discharges part 1: NH3, NH2, and NH. *Plasma Sources Sci. Technol.* **32**, 115020 (2023).
- 35. Rapp, D. & Englander-Golden, P. Total cross sections for lonization and attachment in gases by electron impact. I. Positive ionization. *The Journal of Chemical Physics* **43**, 1464–1479 (1965).
- 36. Tarnovsky, V., Deutsch, H. & Becker, K. Cross-sections for the electron impact ionization of NDx (x = 1-3). *International Journal of Mass Spectrometry and Ion Processes* **167–168**, 69–78 (1997).
- 37. Yoon, J. S. *et al.* Cross sections for electron collisions with hydrogen molecules. *Journal of Physical and Chemical Reference Data* **37**, 913–931 (2008).
- 38. Capitelli, M., Ferreira, C. M., Gordiets, B. F. & Osipov, A. I. *Plasma Kinetics in Atmospheric Gases*. vol. 31 (Springer Berlin Heidelberg, Berlin, Heidelberg, 2000).
- 39. Kossyi, I. A., Kostinsky, A. Y., Matveyev, A. A. & Silakov, V. P. Kinetic scheme of the non-equilibrium discharge in nitrogen-oxygen mixtures. *Plasma Sources Science and Technology* **1**, 207–220 (1992).
- 40. Nighan, W. L. Electron Energy Distributions and Collision Rates in Electrically Excited N2, CO, and CO2. *Physical Review A* **2**, 1989–2000 (1970).

41. Carrasco, E., Jiménez-Redondo, M., Tanarro, I. & Herrero, V. J. Neutral and ion chemistry in low pressure dc plasmas of H2/N2 mixtures: routes for the efficient production of NH3 and NH4+. *Physical Chemistry Chemical Physics* **13**, 19561 (2011).

- 42. Gaens, W. Van & Bogaerts, A. Kinetic modelling for an atmospheric pressure argon plasma jet in humid air. *Journal of Physics D: Applied Physics* **46**, 275201 (2013).
- 43. Yang, X. *et al.* Measurements of atoms and metastable species in N2and H2-N2nanosecond pulse plasmas. *Plasma Sources Science and Technology* **31**, 15017 (2022).
- 44. Gordiets, B., Ferreira, C. M., Pinheiro, M. J. & Ricard, A. Self-consistent kinetic model of low-pressure flowing discharges: II. Surface processes and densities of N, H, species. *Plasma Sources Science and Technology* **7**, 379–388 (1998).
- 45. Herron, J. T. Evaluated Chemical Kinetics Data for Reactions of N(2D), N(2P), and N2(A $3\Sigma u+$) in the Gas Phase. *Journal of Physical and Chemical Reference Data* **28**, 1453–1483 (1999).
- 46. Anicich, V. G. Evaluated Bimolecular Ion-Molecule Gas Phase Kinetics of Positive Ions for Use in Modeling Planetary Atmospheres, Cometary Comae, and Interstellar Clouds. *Journal of Physical* and Chemical Reference Data 22, 1469–1569 (1993).
- 47. Wang, W., Snoeckx, R., Zhang, X., Cha, M. S. & Bogaerts, A. Modeling Plasma-based CO 2 and CH 4 Conversion in Mixtures with N 2, O 2, and H 2 O: The Bigger Plasma Chemistry Picture.

 The Journal of Physical Chemistry C 122, 8704–8723 (2018).
- 48. Clyne, M. A. A. & Stedman, D. H. Rate of recombination of nitrogen atoms. *J. Phys. Chem.* **71**, 3071–3073 (1967).
- 49. Davidson, D. F., Kohse-Höinghaus, K., Chang, A. Y. & Hanson, R. K. A pyrolysis mechanism for ammonia. *International Journal of Chemical Kinetics* **22**, 513–535 (1990).

50. Altinay, G. & Macdonald, R. G. Determination of the Rate Constants for the NH2(X2B1) + NH2(X2B1) and NH2(X2B1) + H Recombination Reactions in N2 as a Function of Temperature and Pressure. *J. Phys. Chem. A* **119**, 7593–7610 (2015).